5-2017

# Characterization of Mixed N,S Donor Ligand and Group 12 Metal Complexes with X-Ray Crystallography, ESI-MS, and NMR

Mikhaila D. Ritz
*College of William and Mary*

Characterization of Mixed N,S Donor Ligand and Group 12 Metal Complexes with X-Ray Crystallography, ESI-MS, and NMR

A thesis submitted in partial fulfillment of the requirement
for the degree of Bachelor of Science in Chemistry from
The College of William and Mary

by

Mikhaila Desmond Ritz

Accepted for _____

_____
Professor Deborah Bebout

_____
Professor Sarah Day

_____
Professor William McNamara

_____
Professor Robert Pike

Williamsburg, VA
May 4, 2017

**Table of Contents**

**Acknowledgements**

First and foremost, I would like to thank Dr. Bebout for all of the knowledge she has imparted. Working in her lab has been a truly wonderful experience, and she has been a great mentor throughout my time here at William and Mary. Additionally, I would like to thank Dr. Day, Dr. McNamara, and Dr. Pike for agreeing to be a part of my panel and taking the time out of their day to do so. Lastly, to my friends and family, thank you for all of your encouragement and support, my sanity is intact because of you all.

## List of Figures

## List of Figures (Continued)

## List of Tables

## Abstract

Group 12 metal ion complexes of mixed N,S donor ligands N-(2-mercaptoethyl) picolylamine (**L**) and N-(2-pyridylmethyl)-N-(2-(methylthio)ethyl)-N-(2-thioethyl)-amine (**L′**) were studied. Characterization of the known complex ion $[Zn(Zn\mathbf{L}_2)_2]^{2+}$ was complemented by X-ray crystallography of a new acetonitrile solvate of the perchlorate salt, ESI-MS and variable temperature NMR studies. In addition, five solvates of the novel alkylthiolate bridged mixed metal complex $[Hg(Zn\mathbf{L}_2)_2](ClO_4)_2$ were formed through either indirect and direct methods. Further characterization of the mixed metal complexes was done through variable temperature NMR, ESI-MS and X-ray crystallography. In addition, an unusual bicyclo spiro [5.5] complex with formula $[Zn((Zn\mathbf{L'})_2(\mu\text{-}OH))_2](ClO_4)_4$ was prepared and characterized by X-ray crystallography. Characterization of this complex in acetonitrile solution by variable temperature NMR and ESI-MS studies indicated possible formation of a $(Zn\mathbf{L'})_4^{+4}$ macrocycle as observed for Hg(II) with **L′**, but no evidence for the carbonate complexes formed by Cd(II) with **L′**.

# Characterization of Mixed N, S Donor Ligand and Group 12 Metal Complexes with X-Ray Crystallography, ESI-MS, and NMR

## Introduction

Biological environments require a complex interplay between organic and inorganic components. The role of metal ions within biological systems is crucial to understand. Many important processes that occur within living systems involve metal ions such as: stabilizing nucleic acid and protein structures, catalyzing enzyme reactions, signal transduction, muscle contraction, hormone secretion, taste and pain sensation, respiration, and photosynthesis. Significantly, metal ions are estimated to be required cofactors for roughly 30% of all proteins, contributing to their catalytic activity and/or structural integrity.[1] Currently, thirteen metals are known to be essential for plants and animals; potassium, calcium, magnesium, and sodium are present in bulk, while vanadium, chromium, molybdenum, manganese, iron, cobalt, copper, nickel, and zinc are found in trace amounts.[2] The concentrations of these metal ions are highly regulated as they can be toxic if their concentrations significantly exceed required amounts. In order to mediate this toxicity, proteins exploit the ability to bind with these metals and use them for their own specific functions.[2]

As crucial as it is to understand the biological interactions between metals and proteins, their complexity can make them challenging to examine in a laboratory setting. Small synthetic metal complexes modeled after protein metal sites provide an alternative amenable to detailed study.[3] It is important to note that synthetic complexes have created the foundation for understanding structural and functional relationships in metalloproteins, as well as uncovering the role of metal ions in biological catalytic pathways. While these small synthetic complexes cannot reproduce the entirety of metal binding frameworks, they provide a stepping stone for truly understanding more complex biological models.

The inspiration for our current research with multidentate thiolate ligands has primarily stemmed from the interaction of Hg(II) and metallothionein. Metallothioneins are a family of cysteine rich proteins found in diverse taxonomic groups that have a variety of different properties.[4] They are most commonly associated with Zn(II) and Cu(I) homeostasis and the detoxification of heavy metals, Hg(II) and Cd(II), throughout the body by using the sulfur in the cysteines to bind to these specific metals. However, in recent years, additional metallothionein protein sequences have become available and experiments have provided evidence for the involvement of histidine nitrogen in the metal-binding process for some sequence variants. Metallothionein protein sequences containing histidine residues in the metal-binding process have been found in a variety of plants and animals, a few examples include: Baker's yeast, Anthracnose fungus, chicken, as well as many different species of cyanobacteria and proteobacteria.[5] The structure of this protein has been best characterized bound to a total of seven metals separated into one-three and one-four metal cluster with each metal bonded to four cysteine thiolate groups. However, a variety of other homo and hetero metal-bound forms likely coexist.[6] Although the first crystal structure of metallothionein was in the form $Cd_5Zn_2$ metallothionein isoform II from rat liver found, all other crystal structures that have been characterized are homometallic.[7]

In particular, our interest lies with the bonding of Hg(II) to metallothionein. Metallothionein has been associated with mercury detoxification, however, there are no crystal structures documenting how Hg(II) binds to the protein. In order to gain information about the relationship between mercury and metallothionein, there have been several recent papers focusing on this topic. Based on previous research suggesting that methylmercury poisoned rats had decreased MDA and urinary mercury levels after a sodium selenite treatment,[8] Li et al.

found that methylmercury poisoned rats had elevated levels of mercury in their protein serum samples after being given a selenium treatment. Through the use of size exclusion chromatography and ICP-MS, three mercury and two selenium binding proteins were identified. Additionally, through the use of MALDI-TOF-MS, the authors were able to analyze the protein serum and found that a fraction was methylmercury binding to metallothionein. While this experiment focuses on organomercury unlike our research, the point is that while we have ample information pointing us towards the idea that mercury does bind to metallothionein, there is still no crystallographic evidence.

Another recent study proposed a strategy for dual detection of both metallothionein and mercury by using a functional chimera aptamer (FCA) designed to form an intact G-quadruplex DNAzyme demonstrating peroxidase-like activities upon hemin binding.[9] Tang et al. hypothesized that there would be a change in color and absorbance corresponding to an alteration in structure of the FCA based on the presence of mercury and metallothionein. Using UV-Vis absorption spectroscopy, they found that upon addition of mercury into the solution of the G-quadruplex the absorption of the catalytic activity plummeted. This observation was consistent with a mercury-facilitated conformational change within the FCA. Following the addition of metallothionein, the absorption signal significantly increased indicating reversion of the G-quadruplex back to its orginal form. The higher binding affinity of metallothionein for Hg(II) than FCA, created a novel way to detect both mercury and metallothionein.

A recent study that further supports a correlation between mercury binding with metallothionein looked at the identification of mercury and other metal complexes with metallothionein in dolphin liver.[10] The liver homogenate from the white-sided dolphin was

analyzed using hydrophilic interaction LC (HILIC) to separate the metallothionein complexes and electrospray high resolution MS to identify the complexes by mass. Upon analysis of the spectra, Pedrero and coworkers found that Hg(II) bound to metallothionein in the form MT-$Zn_6Hg$. In order to conclusively state that this was indeed true, the group spiked the solution with excess Hg(II). When comparing the two spectra, spiked and non-spiked, it was clear that the mercury-metallothionein peak had grown, confirming their peak assignment.

Typically, the synthetic approach of self-assembly is used in order to make metal clusters similar to those found in metallothionein. Inspired in part by the recent discovery of metallothionein forms using both cysteine thiolates and histidine nitrogen for metal binding, our approach uses multidentate mixed donor ligands containing alkylthiolates and nitrogen donors that are able to act, respectively, as the bridging and non-bridging synthetic counterparts of the metal binding groups found in metallothionein. The mixed N, S donor ligand used, containing an alkyl thiolate analogous to the metal-binding side chain of cysteine, was N-(2-mercaptoethyl) picolylamine (**L**) (Figure 1). Ligand **L** was previously used by the Bebout lab to form a novel complex with a bicycle [3.3.3]$Hg_5S_6$ core. This crystallized from a solution with a variety of Hg:L stoichiometries analogous to the physical sequestration of mercury in the kidneys by metallothionein.[11] Futhermore, this complex shares some structural features with the structurally characterized metal clusters of metallothionein such as bicyclic ring structures, thiolate linkages between pairs of metal ions, and four coordinate metal centers.

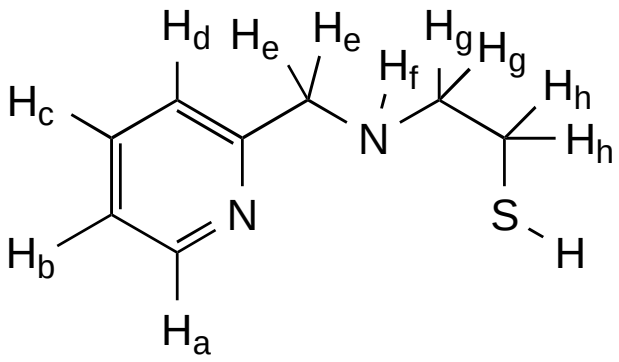


**L**

**Figure 1.** N-(2-Mercaptoethyl) picolylamine with proton labeling (**L**)

The Zn(II) coordination chemistry of **L** has previously been examined by two groups. Brand and Vahrenkamp found that Zn(II) complex of **L** varied structurally depending on the salt used.[12] With counterions commonly described as non-coordinating counterions, they isolated complexes with composition $[Zn_3\mathbf{L}_4](X)_2{\cdot}2H_2O$ ($X= ClO_4^-$, $BF_4^-$, $NO_3^-$) irrespective of the stoichiometric ratio of the reactants. A trinuclear cation, involving two terminal octahedral Zn(II) with $N_4S_2$ coordination bridged by both sulfur atoms to a central tetrahedral Zn(II), was reported for the tetrafluoroborate complex. A methanol solvomorph of the perchlorate complex was characterized by Mikuriya et. al in 1998.[13] Recently an acetonitrile solvomorph of $[Zn_3(\mathbf{L})_4](ClO_4)_2 \cdot 2CH_3CN$ was prepared in our lab (Figure 2).[14] Although the metallothionein three metal cluster is cyclic and this cluster is linear, the unique central site of the linear synthetic cluster was identified as a potential candidate for modeling Hg(II) substitution of a tetraderal thiolate coordinated cluster site. As reported by Brand and Vahrenkamp, the central Zn of this trinuclear complex is in a severely distorted tetrahedral environment which is caused by the

~ 90° S1-Zn1-S1′ angles of the peripheral zinc atoms.[12] Given this distortion and the propensity of Hg to bind with sulfur, the central Zn was anticipated to be the most susceptible to replacement with Hg.

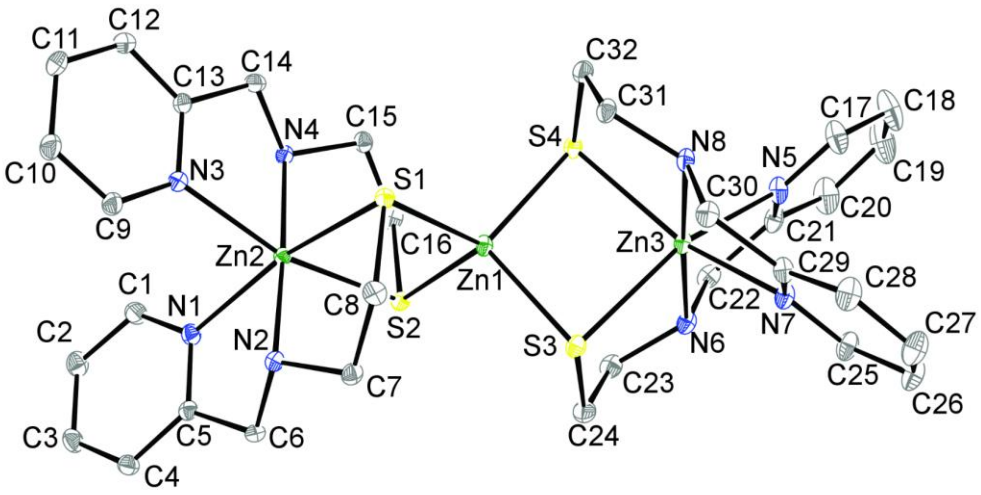


**Figure 2.** $[Zn_3(\mathbf{L})_4](ClO_4)_2 \cdot 2CH_3CN$ (**1c**)

In this work, our focus has shifted to looking at the metal substitution that occurs in metallothionein in the presence of xenobiotic Hg(II). Since we hypothesized that mixed metal metal metallothioneins are formed upon exposure of Zn(II)-metallothionein to Hg(II), we checked the Cambridge Crystallographic data base for examples of alkylthiolated bridged mixed metal complexes. A limited number of structurally characterized mixed metal ZnHg complexes were found, none of which contained alkylthiolate bridges. One of the more relevant structurally characterized complexes was {[μ-N,N′-bis(salicylidene)-2,2′-dimethyl-1,3-propanediaminato](dimethylformamide)zinc(II)}diiodomercury(II) (Figure 3a).[15] Arici and Ülkü found that this novel complex had a hetero-dinuclear metal center made up of Zn and Hg. The coordination around the zinc metal ion is characterized as a distorted square pyramidal with two bridging oxygens and two nitrogen atoms from the ligand in the equatorial plane and one nitrogen from the solvent DMF in the axial position. The mercury metal center has a

coordination geometry that is distorted tetrahedral from two bridging ligand oxygens and two non-bridging iodine atoms. It was classified in the monoclinic system with a space group of P21/*n*. This complex was made to investigate how dinuclear homo- or heterometal complexes with double oxygen-bridges have subnormal magnetic moments because of super-exchange occurring between the bridged metal ions.

Two other mixed metal ZnHg complexes were made by Rombach and Vahrenkamp to explore the nucleation of metal ions around sulfide ions.[16] They used a bulky pyrazoylborate, (Tp= pyrazoylborate with a phenyl and methyl in 3, 5 substituted positions), to encapsulate the zinc ions, making very stable and accessible zinc-hydrosulfide complexes. With benzylmercury bis(trimethylsiyl) amide as the source of mercury, a mixed metal complex was prepared with a nearly right angle, 93.41°, in the Zn-S-Hg unit and an S-Hg-C bond angle of 176.3° (Figure 3b). Benzylmercury bis(trimethylsiyl) amide was also used as the source of Hg(II) to prepare a complex with a pair of sulfide bridges to a pair of [Zn(Tp)] units (Figure 3c). In this complex, the Hg-S-Zn angles were 12° larger, a difference suggested to be due steric congestion.

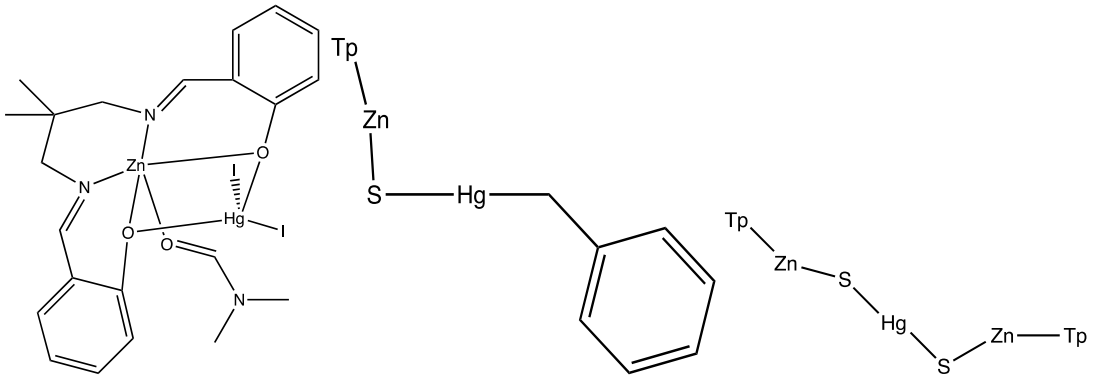


**a)** **b)** **c)**

**Figure 3.** Illustrations of the three relevant ZnHg complexes from literature

Mixed metal ZnHg complexes with bridging alkylthiolate ligands would be more clearly relevant to metallothionein. The seven divalent metal ions present are bound in two separate

clusters, a $M_4S_5$ α-domain (cluster A) and an $M_3S_3$ β-domain (cluster B), as characterized through both NMR or X-ray crystallography experiments. Recent studies have suggested that these metal clusters enable different binding equilibria between metallothionein and its protein target, thus contributing to its dual function of heavy metal detoxification and Zn(II) transfer. However, working with metallothionein as an entire protein can be quite complex and difficult to do in a lab setting. Therefore, the creation of synthetic metal clusters, analogous to those in metallothionein, is important because it allows for more detailed study of the metal exchange process. Additionally, while the malleability of small synthetic clusters of group 12 metal ions is potentially a shortcoming for the modeling of proteins with a single well-defined functional conformation, metallothionein is known to exist in a variety of conformations so the detailed characterization of a variety of closely related complexes is potentially advantageous.

In this work, two different methods for making the desired mixed metal complex were investigated. One way was self-assembly or the direct method, which involves adding all the necessary reagents together in varying stoichiometries. The other was the indirect method, in which one or more Zn(II) is replaced by Hg(II) in a previously made complex of $Zn_3L_4(ClO_4)_2$. In our attempts to recrystallize the mixed metal complex, we were successful in generating solvomorphic crystals of $[Hg(Zn\mathbf{L})_2](ClO_4)_2$ in five different crystal classes. Single crystal X-ray crystallography and powder diffraction was used to characterize and determine the structure of the newly formed solvomorphs. ESI-MS and proton NMR were additional techniques used to help understand the metal substitution process occurring.

In related work, the Zn(II) coordination chemistry of mixed N,S donor ligand N-(2-pyridylmethyl)-N-(2-(methylthio)ethyl)-N-(2-thioethyl)-amine (**L′**, Figure 4) was also investigated. A pentanuclear cluster of Zn(II) with unusual architecture was isolated and

characeterized by single crystal X-ray crystallography. Variable temperature proton NMR studies were used to investigate the integrity of this complex in acetonitrile solution for comparison with previously isolated Cd(II) and Hg(II) complexes.

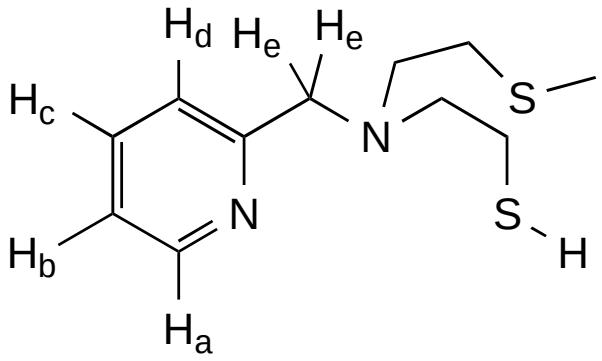


**L′**

**Figure 4.** Structure of N-(2-pyridylmethyl)-N-(2-(methylthio)ethyl)-N-(2-thioethyl)-amine (**L′**) with proton labeling.

Our investigations have led to preparation and characterization of several solvates of novel alkylthiolate-bridged molecular clusters of group 12 metal ions. Reported here are the syntheses of the ligands used metal complexes, the results of the analytical tests done, as well as comparisons to other relevant molecules that help supplement what has been found. These unique structures provide potential insight into the biologically relevant subject of metallothionein metal substitution and the process of heavy metal detoxification. In addition, these studies show that mixed N,S donor ligands can be used to prepare complexes with unusual structures.

## Experimental

### Methods and Materials

Organic reagents and solvents of commercial grade were used as received. Metal salts were dried under vacuum overnight and stored in a desiccator. Capillary melting points were gathered through the use of a Mel-Temp apparatus and are uncorrected. All elemental analyses were done by Atlantic Microlabs, Inc. of Norcross, GA.

**WARNING:** While the perchlorate complexes included in these experiments were stable for the subsequent routine synthesis and purification procedures, caution should be implemented as perchlorate salts of metal complexes with organic ligands are potentially explosive.[17]

### Instrumental Procedures

### X-Ray Diffraction

Single crystals were harvested and then attached to a glass fiber. Data was collected using a Bruker SMART Apex II three-circle diffractometer system with graphite monochromator, Cu Kα fine-focus sealed tube (λ = 1.54178 Å), and CCD collector using φ and ω scans. The sealed tube source used was either Cu Kα fine-focus (**1c, 2f** ) or microfocus (**2a**) (λ= 1.54178 Å) or Mo Kα fine-focus (λ=0.71073 Å) (**2c, 2d**). SADABS was then used to correct the collected data for Lorentz and polarization effects in addition to absorption. Direct methods were used to solve the structures. Structures were refined on $F_2$ by full-matrix least squares with the use of the SMART Apex and SHELX14 program package. Additionally, all non-hydrogen atoms were refined anisotropically, while the hydrogen atomic positions on the bonded carbons were fixed isotropically with regards to thermal parameters.

The CCDC program *Mercury*, version 1.4.2, was used to indicate geometrical parameters in order to detail the stacking interactions between pyridine rings. This specific version was used, as some of the newer ones lack the function to calculate normal projection distances between centroids and planes.

**Powder Diffraction**

Powder diffraction analysis was carried out using the instrument described above. The samples were ground up using a mortar and pestle and then mixed with Parabar 10312 oil to create a mull. Collection of four 180s frames covering 8-100° 2θ were merged using the SMART Apex II software. Further processing was done with the use of Diffrac-EVA software.

**Solution-State NMR Spectroscopy**

Using an Agilent 400-MR DD2 NMR spectrometer operating in the pulse Fourier transform mode, proton NMR spectra were collected on samples in 5mm o.d. NMR tubes. Variable temperature NMR measurements were taken on samples nominally 0.5-5.0 mM made using of calibrated autopipets. In order to maintain the sample temperature, chilled nitrogen was blown over the NMR tube in the probe. Over extended periods of time, the solution NMR spectra were found to be stable. Additionally, coupling constants are reported with Hertz for units and proton chemical shifts were measured with respect to their internal solvent but reported relative to tetramethylsilane (TMS).

## Syntheses

### Synthesis of N-(2-Mercaptoethyl)picolylamine (L).

Literature procedures were used to prepare **L**. Colorless distilled **L** was stored refrigerated and handled under argon to limit air oxidation. $^{1}$H NMR ($CD_3CN$) δ 8.495 (d, 1H, *J* = 4.7 Hz, $H_a$), 7.689 (ddd, 1H, *J* = 7.9, 7.9 Hz, $^{4}J_{HH}$ = 1.5 Hz, $H_c$), 7.365 (d, 1H, *J* = 7.9 Hz, $H_d$), 7.185 (dd, 1H, *J* = 5.0, 7.6 Hz, $H_b$), 3.831 (s, 2H, $H_e$), 2.767 (s, 2H, *J* = 6.5, $H_g$), 2.612 (s, 2H, *J* = 7.9, $H_h$)

### $[Zn(ZnL_2)_2](ClO_4)_2$ (**1**)

A precipitate of **1** was prepared in quantitative yield by the method Brand & Vahrenkamp.[13] Mp 200 ºC (dec.). $^{1}$H NMR (nominally 2 mM, $CD_3CN$, 20 ºC δ 8.070 (d, 1H, *J* = 4.9 Hz, $H_a$), 7.949 (ddd, 1H, *J* = 7.8, 7.8 Hz, $^{4}J_{HH}$ = 1.3 Hz, $H_c$), 7.517 (d, 1H, *J* = 7.7 Hz, $H_d$), 7.344 (dd, 1H, *J* = 5.5, 7.8 Hz, $H_b$), 4.428 (dd, 1H, *J* = 5.1 Hz, $^{2}J$ = 15.5 Hz, $H_e$), 4.001 (dd, 1H, *J* = 11.8 Hz, $^{2}J$ = 14.8 Hz, $H_{e'}$), 3.409 (m, 1H, $H_h$), 3.376 (m, 1H, $H_f$), 3.052 (dddd, 1H, *J* = 3.25, 12.0, 12.0, 12.0, $H_{g'}$), 2.969 (d, 1H, *J* = 13.81, $H_{h'}$), 2.495 (ddd, 1H, *J* = 3.24, 13.26, 13.26, $H_g$). Anal. Calcd for $C_{32}H_{44}Cl_2N_8O_8S_4Zn_3$: C 36.11; H 4.17; N 10.54. Found: C 36.27; H 4.20; N 10.49 %.

### $[Zn(ZnL_2)_2](ClO_4)_2 \cdot 2CH_3CN$ (**1c**)

Recrystallization of $[Zn_3(\mathbf{L})_4](ClO_4)_2$ (50 mg, 44μmol) from acetonitrile/toluene by slow evaporation provided **1c** (8.4mg, 7.3μmol, 17%). NMR identical to **1**. Mp 177 ºC (dec). Anal. Calcd for $C_{36}H_{50}Cl_2N_{10}O_8S_4Zn_3$: C 37.72; H 4.40; N 12.23. Found: C 37.91; H 4.44; N 12.20 %

**$[Hg(ZnL_2)_2](ClO_4)_2$ (2)**:

A mixture of $Zn(ClO_4)_2 \cdot 6H_2O$ (485 mg, 1.3 mmol) and $Hg(ClO_4)_2 \cdot 3H_2O$ (295 mg, 0.65 mmol) in 15 mL water was added dropwise over 30 minutes to a solution of NaOH (100 mg, 2.6 mmol) and **L** (436 mg, 2.6 mmol) in 40 mL of water. A white solid started forming about halfway through addition of the metal mixture. The suspension was stirred briefly. A white solid was collected by vacuum filtration dried under vacuum overnight. The anhydrous precipitate was amorphous. A crystalline phase with powder pattern matching **2a** coprecipitated in some preps. $^1$H NMR (nominally 2 mM, $CD_3CN$, 20 ºC) δ $^1$H NMR ($CD_3CN$, 20°C): δ 8.10 (bs, 1H), 7.94 (bm, *J* = 8, 8 Hz, $H_c$), 7.50 (bs, 1H, $H_d$), 7.36 (dd, 1H, J = 8, 5, $H_c$), 4.39 (bs, 1H, $H_e$), 4.05 (bs, 1H, $H_e'$), 3.62-2.57 (bm, 4H, $H_f$, $H_g$, & $H_b$) Yield 426 mg (354 μmol, 54%). Anal. Calcd for the anhydrate $C_{32}H_{44}Cl_2HgN_8O_8S_4Zn_2$: C 32.04; H 3.70; N 9.35. Found: C 31.97; H 3.76; N 9.19 %.

**$[Hg(ZnL_2)_2](ClO_4)_2 \cdot 2H_2O$** (**2a**):

Recrystallization of precipitate **2** (50 mg, 40 μmol) from acetonitrile/toluene by slow evaporation initially provided colorless plates of **2a**. Yield: 15 mg (12 μmol, 30%). M.P. 179 ºC (dec.). $^1$H NMR (nominally 2 mM, $CD_3CN$, 20 ºC) δ 8.085 (m, 1H, $H_a$), 7.953 (dd, 1H, *J* = 7.8, 7.8 Hz, $H_c$), 7.519 (d, 1H, *J* = 7.8 Hz, $H_d$), 7.352 (dd, 1H, *J* = 5.0, 7.8 Hz, $H_b$), 4.421 (dd, 1H, *J* = 4.4 Hz, $^2J$ = 15.2 Hz, $H_e$), 4.015 (dd, 1H, *J* = 11.7, Hz, $^2J$ = 14.7 Hz, $H_{e'}$), 3.5-3.3 (m, 2H, $H_h$ & $H_f$), 3.1-2.9 (m, 2H, $H_{g'}$ & $H_{h'}$), 2.8-2.6 (m, 1H, $H_g$). Anal. Calcd for $C_{32}H_{48}Cl_2HgN_8O_{10}S_4Zn_2$: C 31.12; H 3.92; N 9.07. Found: C 31.05; H 3.92; N 8.95%.

**$[Hg(ZnL_2)_2](ClO_4)_2 \cdot 2CH_3CN \cdot 2(HO_{0.5}) \cdot$ toluene** (**2d**):

Colorless needles of **2d** were grown by further slow evaporation of the **2a** mother liquor or by slow diffusion of an acetonitrile solution of **2** into toluene. The crystals were unstable to loss of solvent, turning opaque after a short time in air. Crystals transferred to oil immediately after removal of mother liquor had sufficient integrity for single crystal diffraction at 100K. NMR same as **2a** with addition of toluene peaks.

**$[Hg(ZnL_2)_2](ClO_4)_2 \cdot 1.5$ toluene** (**2e**):

Very fine colorless needles of **2e** were grown by further slow evaporation of the **2d** mother liquor or by slow diffusion of an acetonitrile solution of **2** into toluene. Crystal quality deteriorated rapidly upon removal of the mother liquor even with immediate transfer to oil. A low resolution structure indicated **2e** crystallized in triclinic *P*-1 (a 9.5764(2); b 17.5637(5); c 17.8334(5);α 111.158(2); β 100.601(2); γ 101.282(2); V 2634.84(13); Z = 2), but was isomorphic with neither **1b** nor **2f**. NMR same as **2a** with addition of peaks for toluene. Anal. Calcd for $C_{35.5}H_{48}Cl_2HgN_8O_8S_4Zn_2$ (corresponding to 0.5 toluene solvate): C 34.23; H 3.89; N 9.00. Found: C 34.41; H 3.85; N 8.83%.

**[HgL($ClO_4$)] (3)**:

An amorphous precipitated of **3** was prepared as reported previously.[12] $^1$H NMR (nominally 2 mM, $CD_3CN$, 20 ºC) δ 8.58 (d, 1H, *J* = 5 Hz, $H_a$), 8.03 (dd, 1H, *J* = 8, 8 Hz, $H_c$), 7.60 (dd, 1H, *J* = 5, 8 Hz, $H_b$), 7.55 (d, 1H, *J* = 8 Hz, $H_d$), 4.33 (bs, 3H, , $H_e$ ,$H_e$), 3.24 (m, 4H, $H_g$, $H_g$). Anal. Calcd for $C_8H_{11}ClHgN_2O_4S$: C 20.56; H 2.37; N 5.99. Found: C 20.82; H 2.33; N 6.00%.

**[Hg($ZnL_2$)$_2$]($ClO_4$)$_2$·$CH_3CN$·0.5toluene** (**2f**):

An acetonitrile solution of **1** (33 mg, 31 μmol) was mixed with an acetonitrile solution of **3** (15 mg, 32 μmol) and diluted with toluene. Colorless crystals of **2f** cocrystallized with **1a** by slow evaporation. Slow diffusion of toluene into 1:1 acetonitrile solution of **1** and **3** into toluene also produced **2f** mixed with **1a** and **2c**.

**[Hg($ZnL_2$)$_2$]($ClO_4$)$_2$·2$CH_3CN$** (**2c**)

Solvate of **2c** was cocrystallized with **2f** and **1a** and **2c** by slow diffusion of a 1:1 acetonitrile solution of **1** and **3** into toluene.

**N-(2-pyridylmethyl)-N-(2-(methylthio)ethyl)-N-(2-thioethyl)-amine** (**L′**)

Literature procedures were used to prepare **L′**.[18] Colorless distilled **L** was stored refrigerated and handled under argon to limit air oxidation. $^1$H NMR ($CD_3CN$, 20°C): δ 8.49 (dm, 1H, J= 5 Hz), 7.73 (td, 1H, J = 8, 2 Hz), 7.55 (d, 1H, J = 8 Hz), 7.22 (dd, 1H, J = 8, 5 Hz), 3.78 (s, 2H), 2.74 (m, 4H), 2.62 (m, 4H), 2.05 (s, 3H).

**$[Zn(Zn(L')_2(\mu\text{-}OH))_2](ClO_4)_4$**

Added **L′** (42 mg, 172 μmol) to an acetone solution where $Zn(ClO_4)_2$ (96 mg, 258 μmol) was added dropwise. Added one equivalent of $NEt_3$ (24 μL, 172 μmol) to solution. Solution was then filtered using celite and then set up for slow diffusion by layering with ether. Yield: 8.1 mg (10%). $^1$H NMR ($CD_3CN$, 20°C): δ 8.75 (m, 1H, J = 5 Hz, $H_a$), 8.12 (m, 1H, $H_c$), 7.60 (m, 2H, $H_b$ & $H_d$), 4.06-3.79 (m, 2H, $H_e$), 3.25-2.595 (m, 7H, ethylene protons), 2.31 (s, ~0.5H, $CH_3$), 2.11 (s, ~0.5H, $CH_3$).

## Results and Discussion

### Overview of Number Scheme and Complex Chirality

Since this work produced a variety of closely related pseudo-polymorphic complexes before delving into the complexities of how each solvate is made and the details of specific bonding, it will be helpful to have a preview of the complexes discussed. As there were so many solvates with slightly different aspects, a naming scheme was adapted to help organize them accordingly. The number indicates whether the complex has a $Zn_3$ metal core (**1**) or $Zn_2Hg$ metal core (**2**). The letter after the number identifies the solvomorph, **a** is $H_2O$, **b** is $CH_3OH$, and etc. A prime was added after the letter to distinguish the one tetrafluoroborate salt from the perchlorate salts. Complexes **1a′** and **2a** crystallized in *I*-4 and were isomorphic, while the other complexes had distinctive unit cells. Since the meridional bis-tridentate chelates exhibited chirality, the molecular chirality of each complex is also provided in Table 1.

**Table 1.** Numbering Scheme for Pseudo-polymorphic Complexes

| Number | Composition | Molecular Chirality[1,2] | Ref. |
|---|---|---|---|
| **1a′** | $[Zn(Zn\mathbf{L})_2](BF_4)_2\cdot 2H_2O$ | Meso $\Delta\Lambda$[2] | 12 |
| **1b** | $[Zn(Zn\mathbf{L})_2](ClO_4)_2\cdot 2CH_3OH$ | Pseudo-meso $\Delta\Lambda$[1] | 13 |
| **1c** | $[Zn(Zn\mathbf{L}_2)_2](ClO_4)_2\cdot 2CH_3CN$ | Pseudo-meso $\Delta\Lambda$[1] | This work |
| **2a** | $[Hg(Zn\mathbf{L}_2)_2](ClO_4)_2\cdot 2H_2O$ | Meso $\Delta\Lambda$[2] | This work |
| **2c** | $[Hg(Zn\mathbf{L}_2)_2](ClO_4)_2\cdot 2CH_3CN$ | Pseudo-meso $\Delta\Lambda$[1] | This work |
| **2d** | $[Hg(Zn\mathbf{L}_2)_2](ClO_4)_2\cdot 2CH_3CN\cdot 2(HO_{0.5})\cdot$toluene | Racemic $\Delta\Delta/\Lambda\Lambda$[1] | This work |
| **2e** | $[Hg(Zn\mathbf{L}_2)_2](ClO_4)_2\cdot 1.5$toluene | Racemic $\Delta\Delta/\Lambda\Lambda$[1] | This work |
| **2f** | $[Hg(Zn\mathbf{L}_2)_2](ClO_4)_2\cdot CH_3CN\cdot 0.5$toluene | Pseudo-meso $\Delta\Lambda$[1] | This work |

[1] Inversion-related pairs observed; [2] Pair of independent molecules in asymmetric unit.

Meso ΔΛ ΔΔ Diastereomers ΛΛ

**Figure 5.** Schematic depiction of the meso and diastereomeric configuration

**Synthetic Methods**

Using established methods, an initial precipitate of the complex $[Zn_3\mathbf{L}_4](ClO_4)_2$ (**1**) was prepared from water.[13] Recrystallization of (**1**) through the method of slow evaporation with toluene/acetonitrile resulted in the preparation of new acetonitrile solvomorph, $[Zn(Zn\mathbf{L})_2](ClO_4)_2 \cdot 2CH_3CN$ (**1c**). There were two different approach making the $[Hg(Zn\mathbf{L}_2)_2](ClO_4)_2$ (**2**) complex (Figure 6). For the direct method, the necessary components were added in the appropriate mole ratios for self-assembly. In order to make this specific complex (**2**), an aqueous solution containing a 1:2 mole ratio of $Hg(ClO_4)_2$: $Zn(ClO_4)_2$ was added dropwise to the NaOH deprotonated **L** in a 3:4 metal to ligand stoichiometric ratio. Recrystallization of **2** by slow evaporation from toluene/acetonitrile produced colorless plates of $\mathbf{2} \cdot 2H_2O$ (**2a**), in low yield. Taking the mother liquor from complex **2a** allowed for further crystal growth, producing crystalline needles of another solvate, $\mathbf{2} \cdot CH_3CN \cdot 0.5$ toluene (**2d**). This solvate proved to be unstable as it quickly lost solvent outside of the mother liquor. Further slow evaporation from the mother liquor of complex **2d** produced fine colorless needles of $\mathbf{2} \cdot 1.5$toluene (**2e)**, which were also unstable to loss of solvent. Additionally, we attempted to synthesize an isomorph of the acetonitrile solvate, **1c**, through slow diffusion of ether into an acetonitrile solution of precipitate **2a**. Unfortunately, the colorless needles produced appeared to be a solvomorphic variant of **2d** in which toluene was replaced with disordered acetonitrile and

ether (**2g**; data not shown). Additionally, the attempted preparation of complexes with alternative Zn:Hg:**L** ratios by direct syntheses did not provide any promising materials based on NMR or elemental analysis results.

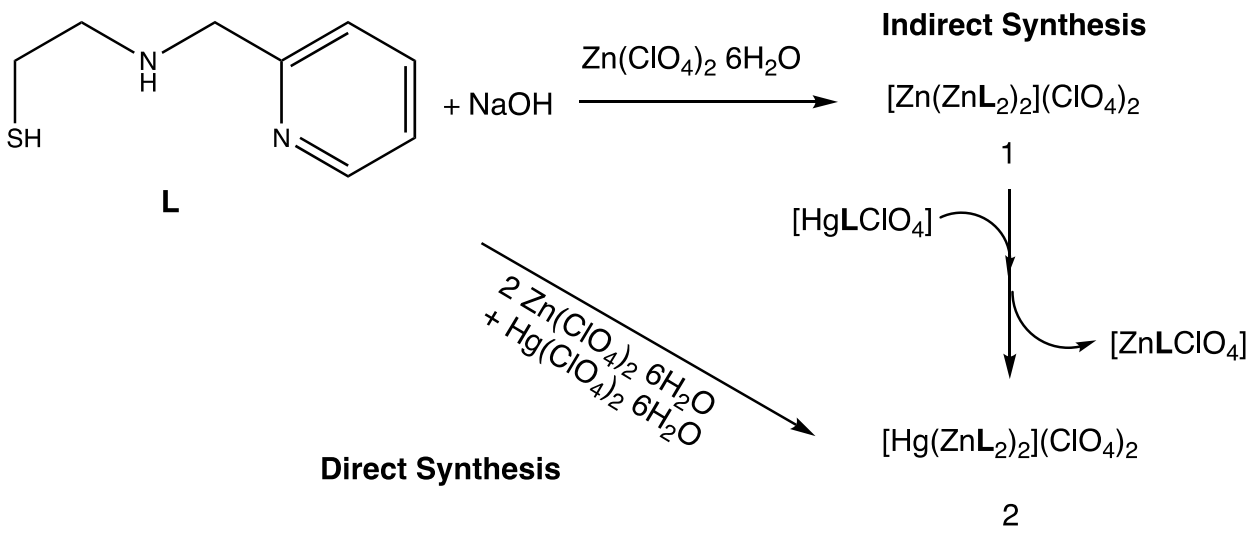


**Figure 6.** Schematic detailing the two different ways to make $[Hg(Zn\mathbf{L}_2)_2](ClO_4)_2$

Additional solvates of $[Hg(Zn\mathbf{L}_2)_2](ClO_4)_2$ were prepared through an indirect synthesis. In this method, one equivalent of$[Hg\mathbf{L}(ClO_4)]$ (**3**) was added to the precipitate of **1** in acetonitrile and diluted with toluene. At first, plates of **2**·$CH_3CN$·0.5toluene (**2f**) and **1c** were formed in trace amounts in addition to non-diffracting solids. Upon layering the saturated solution on toluene for slow diffusion, higher quality crystals **2f**, as well as plates of **2**·$2CH_3CN$ (**2c**), were formed.

**Solution and Gas Phase Characterization (NMR, MS)**

Previously reported NMR experiments on $[Zn(Zn\mathbf{L})_2](BF_4)_2 \cdot 2H_2O$ (**1a′**) were done in a highly polar solvent, DMSO, which caused broadening in the spectra.[13] Because of this, little information other than showing the presence of certain constituents was provided. However, the $^1$H NMR of **1c** in dry $CD_3CN$ exposed a prominent ligand environment with ten resolved major resonances (Figure 7). The geminal coupling of the methylene protons is consistent with a tridentate chelate structure and ligand in slow exchange on the coupling constant time scale. Additional minor resonances with poorly resolved splitting were observed in the proton NMR of both precipitated **1** and recrystallized **1c** in dry $CD_3CN$ at 20 ºC (Figure 7b). Upon cooling to -40 ºC, the intensities of these features shrank (Figure 7b), which suggests the major species could undergo temperature dependent thermal fragmentation. Furthermore, upon increasing the temperature to 60 ºC (Figure 7a), a single set of broadened resonances was observed for the ligand protons. There was a loss of the geminal splitting at elevated temperature, thus suggesting that the intermolecular exchange processes were becoming rapid on the chemical shift time scale.

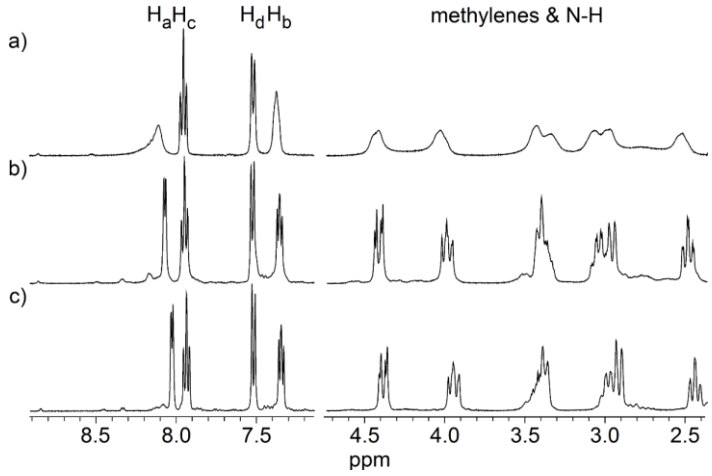


**Figure 7.** Variable temperature proton NMR of **1c**. a) 60 °C. b) 20 °C. c) -40 °C.

When doing the same VT NMR experiment with the $[Zn_2Hg\mathbf{L}_4]^{2+}$ complexes we were able to see four downfield pyridyl proton resonances and seven distinguishable upfield protons with extensive geminal splitting were seen (Figure 8). The appearance of geminal splitting indicates that the geminal protons are locked into different environments on the coupling constant time scale, which is a good indicator that the ligands are indeed attached to the metals. Futhermore, the $H_a$ resonance had a shoulder suggesting a second environment. This shoulder became more pronounced and the other resonances became more complex as the temperature was lowered to -40 ºC (Figure 8c). This NMR behavior is consistent with slow exchange between the enantiomers of **2**. A second ligand environment with comparable mole fraction was not observed for **1**, possibly because one enantiomer was considerably more stable than the other or because of insufficient chemical shift dispersion for the homometallic enantiomers. At elevated temperatures, the peaks of **2** broadened considerably, which suggests that the intermolecular exchange processes were becoming more rapid. The broadening observed at higher temperatures was larger for that of $[Zn_2Hg\mathbf{L}_4]^{2+}$ than for $[Zn_3\mathbf{L}_4]^{2+}$, which could be due to either the greater complexity of solution equilibria for $[Zn_2Hg\mathbf{L}_4]^{2+}$ or relative exchange rates more closely matched to the coupling and chemical shift time scales.

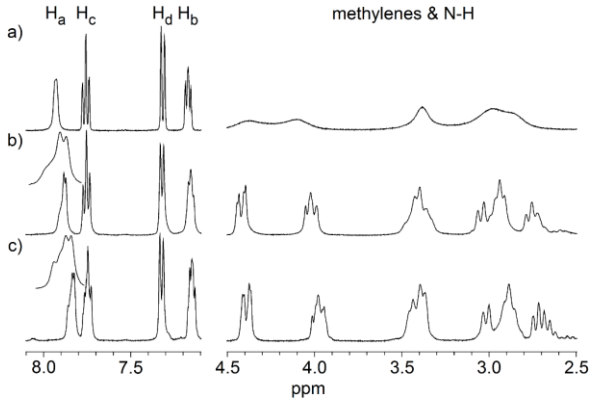


**Figure 8.** Variable temperature proton NMR of **2d**. a) 60 °C. b) 20 °C. c) -40 °C

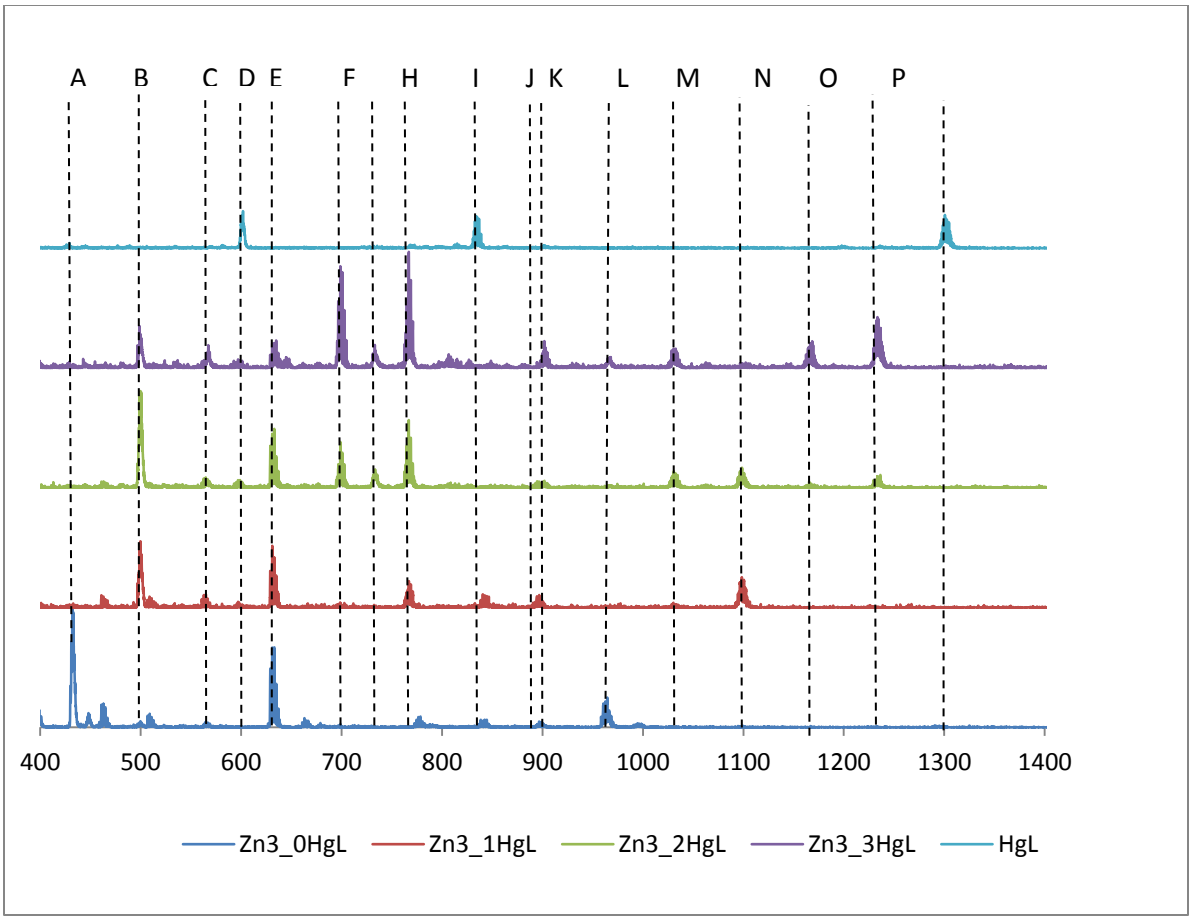


**Figure 9.** ESI-MS of $[Zn_3\mathbf{L}_4(ClO_4)_2]\cdot 2CH_3CN$ (**1c**), $[Hg\mathbf{L}(ClO_4)]$ (**3**) and mixtures of the two. a) **3**, b) 1:1 **1c**:**3**, c) 1:2 **1c**:**3**, d) 1:3 **1c**:**3**, e) **1c**. Labeled peak assignments with X = $ClO_4$ (average *m/z*): A $[Zn_3\mathbf{L}_4]^{2+}$ (432); B $[HgZn_2\mathbf{L}_4]^{2+}$ (500); C $[Zn_2\mathbf{L}_2X]^{+}$ (565); D $[Hg_3\mathbf{L}_3X]^{2+}$ (601); E $[Zn_2\mathbf{L}_3]^{+}$ (632); F $[HgZn\mathbf{L}_2X]^{+}$ (699); G unassigned; H $[HgZn\mathbf{L}_3]^{+}$ (767); I $[Hg_2\mathbf{L}_2X]^{+}$ (836); J $[Zn_3\mathbf{L}_3X]^{+}$ (896); K $[Hg_2\mathbf{L}_3]^{+}$ (902); L $[Zn_3\mathbf{L}_4X]^{+}$ (960); M $[HgZn_2\mathbf{L}_3X_2]^{+}$ (1035); N $[HgZn_2\mathbf{L}_4X]^{+}$ (1099); O $[HgZn_2\mathbf{L}_5]^{+}$ (1167); P $[Hg_2Zn_3\mathbf{L}_4X_2]^{+}$ (1233); Q $[Hg_3\mathbf{L}_3X_2]^{+}$ (1303).

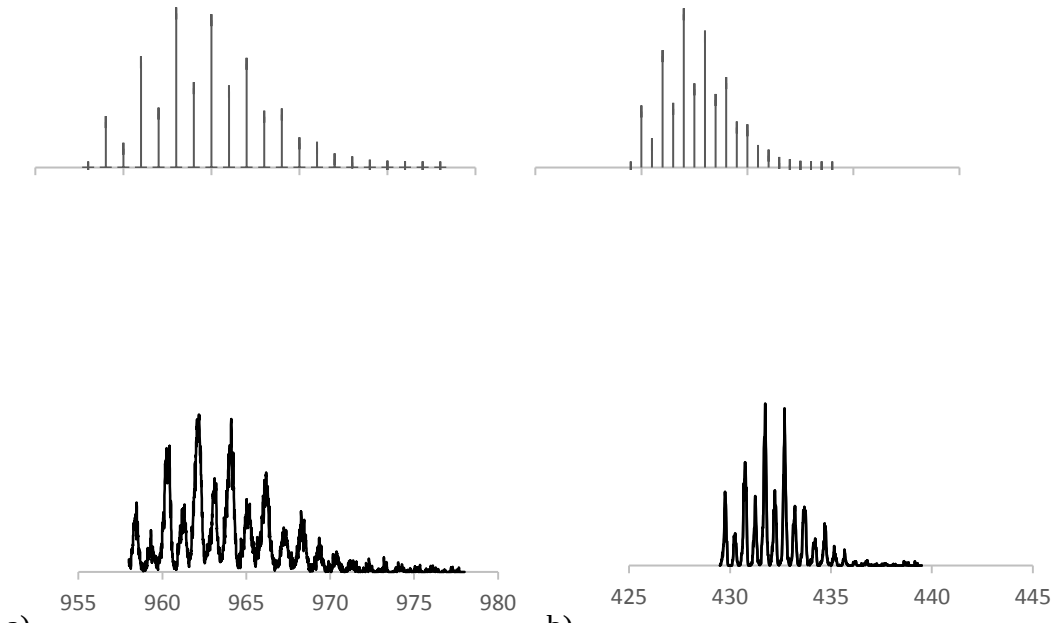


**Figure 10.** Comparison of the experimental (top) and theoretical (bottom) isotope patterns for a) $[Zn_3\mathbf{L}_4ClO_4]^+$ and b) $[Zn_3\mathbf{L}_4]^{2+}$.

In order to further characterize **1**, ESI-MS was used (Figure 9 and 10). The experimental spectrum had an ion cluster with an average *m/z* of 432 corresponding to $[Zn_3\mathbf{L}_4]^{2+}$as its base peak. Other major ion clusters corresponded to $[Zn\mathbf{L}]^+$ (average *m/z* 232, not shown) and $[Zn_2\mathbf{L}_3]^+$ (average *m/z* 632), likely formed by fragmentation of $[Zn_3\mathbf{L}_4]^{2+}$. We were also able to determine that the intact complex was formed, $[Zn_3\mathbf{L}_4ClO_4]^+$, which had an ion cluster with an average *m/z* of 960. Comparison of the theoretical with experimental isoptope patterns confirmed assignments (Figure 10). Note that a direct relationship between ion intensities and solution concentrations cannot be assumed since ions due to differences in transfer efficiency of ions to the gas phase and ion stability.

The ESI-MS spectrum for $[HgZn_2\mathbf{L}_4](ClO_4)_2$ (**2**) had several assignable ion clusters of varying intensity (Figure 11). Diverse ESI-MS speciation for complexes of **L** with metal:ligand ratio lower than one was previously observed for $[Hg_5\mathbf{L}_6](ClO_4)_2$.[12] Again, it is important to note that the intensity of the MS peak and the abundance of the ion within solution are not correlated as intensities deal with how easily something becomes ionized and transferred to the gas phase. Additionally, because ESI-MS is a soft ionization technique and does not forcefully break apart the complex into ions, whatever is shown in the spectra, must be in the solution as well. Therefore, because we see these ions of the family $Hg_xZn_y\mathbf{L}_z^{+n}$, they must also be in solution. In addition, a titration experiment was carried out starting with a solution of **1** and adding up to 3 equivalents of $[Hg\mathbf{L}ClO_4]$ (**3**) (Figure 9b-d). With the addition of **3**, peaks corresponding to **2** and other mixed metal complexes increased in intensity as the ratio of **3**:**1** was increased. Interestingly, no peaks for **2** were observed by ESI-MS when $Hg(ClO_4)_2$ was added to **1** (data not shown).

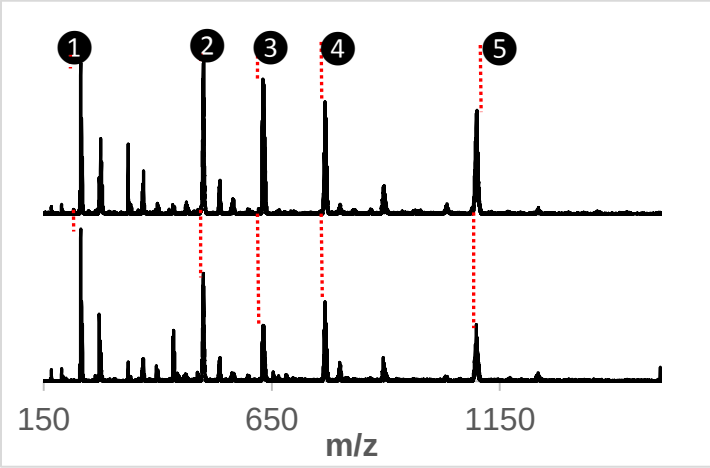


**Figure 11.** Comparison of $[HgZn_2\mathbf{L}_4](ClO_4)_2$ precipitate **2** made two different times showing the reproducibility in ESI-MS spectra. Labeled peak assignments with X = $ClO_4$ (average *m/z*): ❶ $[Zn\mathbf{L}]^+$ (231); ❷ $[HgZn_2\mathbf{L}_4]^{2+}$ (500); ❸ $[Zn_2\mathbf{L}_3]^+$ (632); ❹ $[HgZn\mathbf{L}_3]^+$ (769); ❺ $[HgZn_2\mathbf{L}_4X]^+$ (1099).

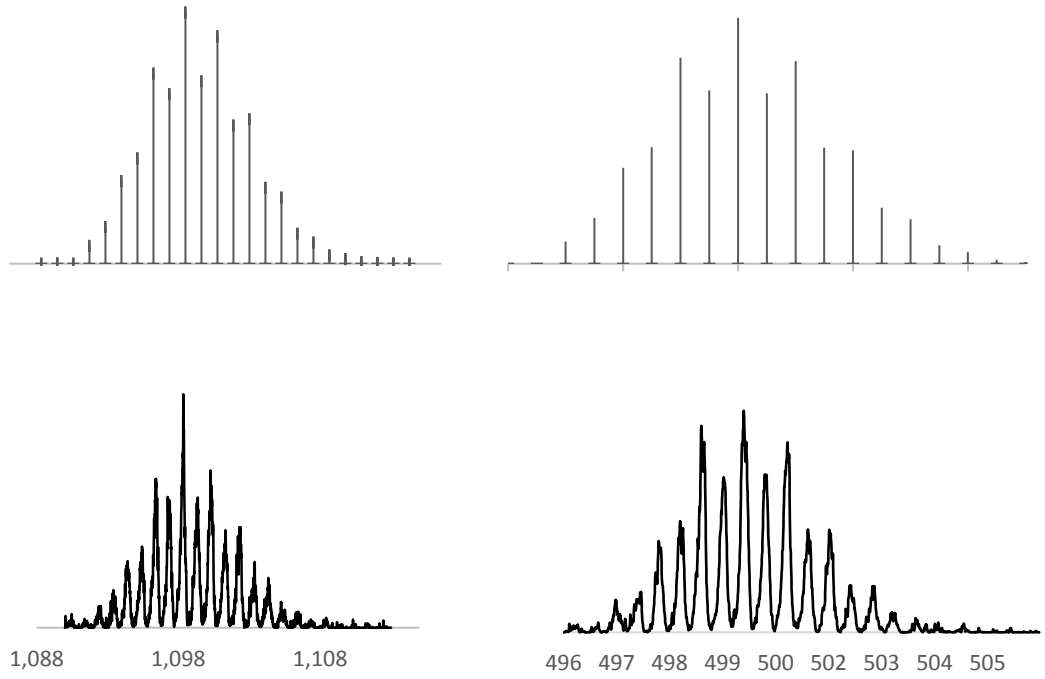


a) b)

**Figure 12.** Comparison of the experimental (top) and theoretical (bottom) isotope patterns for a) $[HgZn_2L_4ClO_4]^+$ and b) $[HgZn_2L_4]^{2+}$

**Crystal Structures**

It has been previously reported that zinc salts of non-coordinating anions will react with sodium hydroxide deprotonated **LH** to produce $[Zn_3\mathbf{L}_4]X_2$ (X = $ClO_4$ (**1**), $BF_4$ (**1′**), $NO_3$).[13] These complexes formed regardless of the stoichiometric ratios of reactants. Crystallographic characterization of the water and methanol solvates, **1a′** and **1b**, indicated a trinuclear metal complex with alkylthiolates bridging between a central tetrahedrally coordinated Zn(II) and two octahedral Zn$\mathbf{L}_2$ units. In contrast, a mix of a 1:1:1 combination of Hg(II):**LH**:NaOH in water formed an amorphous precipitate of the composition [Hg**L**($ClO_4$)].[12]

Recrystallization of $[Zn_3\mathbf{L}_4]\,(ClO_4)_2$ from acetonitrile produced a new solvate $[Zn(Zn\mathbf{L})_2](ClO_4)_2\cdot 2CH_3CN$ (**1c**); it crystallized into the orthorhombic space group $Pna2_1$ as sheets of parallel offset strands. The asymmetric unit of **1c** contains two perchlorates, two acetonitrile solvents, and an asymmetric $[Zn(Zn\mathbf{L})_2]^{2+}$ structurally similar to the complex ions of **1a′** and **1b** (Figure 13a, Table 2). These complex ions are arranged in a head-to-tail manner, forming continuous strands that are linked together in a four-fold embrace (Figure 13b). The two oxygens of one perchlorate bridge complexes through hydrogen bonding between N4 and N8 (Figure 13d, Table 3 (Hydrogen bonding)), thus forming antiparallel offset corrugated sheets (Figure 13c) of the pseudo-meso ($\Delta\Lambda$) complex. Additional hydrogen bonding can be see between N2 and one oxygen of the other perchlorate ion as well, as well as between the amino hydrogen on N6 and one acetonitrile nitrogen (Figure 13d). The homogeneity of this complex has been confirmed through powder diffraction (Figure 14).

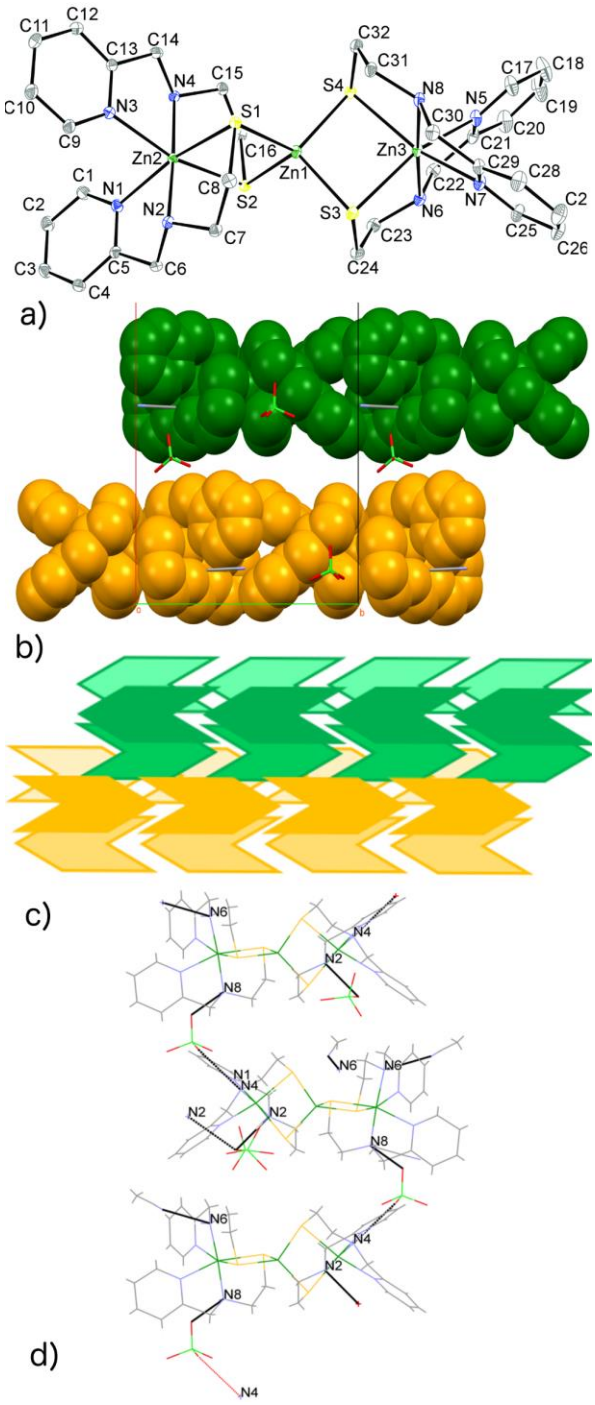


**Figure 13** a) Framework of $[Zn(Zn\mathbf{L})_2](ClO_4)_2 \cdot 2CH_3CN$ (**1c)** with atom number b) Space filling diagram of **1c** to illustrate head-to-tail configuration of two pairs of inversion related complexes c) Schematic packing design for **1c** d) Hydrogen bonding observed in **1c**.

**Table 2.** Selected bond lengths (Å) and bond angles (º) for **1c**

| | | | |
|---|---|---|---|
| Zn1-S1 | 2.3414(8) | Zn1-S3 | 2.3405(7) |
| Zn1-S2 | 2.3383(8) | Zn1-S4 | 2.3506(7) |
| Zn2-S1 | 2.5910(7) | Zn3-S3 | 2.5434(7) |
| Zn2-S2 | 2.5153(7) | Zn3-S4 | 2.5304(7) |
| Zn2-N1 | 2.238(2) | Zn3-N5 | 2.206(2) |
| Zn2-N2 | 2.128(2) | Zn3-N6 | 2.132(2) |
| Zn2-N3 | 2.196(2) | Zn3-N7 | 2.197(2) |
| Zn2-N4 | 2.134(2) | Zn3-N8 | 2.153(2) |
| S1-Zn1-S2 | 101.07(3) | S2-Zn1-S3 | 110.53(3) |
| S1-Zn1-S3 | 113.76(3) | S2-Zn1-S4 | 113.29(3) |
| S1-Zn1-S4 | 116.54(3) | S3-Zn1-S4 | 102.02(3) |
| S1-Zn2-S2 | 90.05(2) | S3-Zn3-S4 | 91.89(2) |
| S1-Zn2-N1 | 160.07(6) | S3-Zn3-N5 | 160.16(7) |
| S1-Zn2-N2 | 83.22(6) | S3-Zn3-N6 | 83.22(7) |
| S1-Zn2-N3 | 92.81(6) | S3-Zn3-N7 | 92.79(7) |
| S1-Zn2-N4 | 98.26(6) | S3-Zn3-N8 | 97.46(7) |
| S2-Zn2-N1 | 96.48(6) | S4-Zn3-N5 | 95.09(7) |
| S2-Zn2-N2 | 98.58(6) | S4-Zn3-N6 | 99.54(6) |
| S2-Zn2-N3 | 83.70(6) | S4-Zn3-N7 | 160.23(7) |
| S2-Zn2-N4 | 83.70(6) | S4-Zn3-N8 | 83.49(6) |
| N1-Zn2-N2 | 77.21(8) | N5-Zn3-N6 | 77.32(9) |
| N1-Zn2-N3 | 87.02(9) | N5-Zn3-N7 | 86.88(9) |
| N1-Zn2-N4 | 101.15(9) | N5-Zn3-N8 | 101.77(9) |
| N2-Zn2-N3 | 100.14(8) | N6-Zn3-N7 | 100.07(9) |
| N2-Zn2-N4 | 177.30(8) | N6-Zn3-N8 | 176.88(9) |
| N3-Zn2-N4 | 77.57(9) | N7-Zn3-N8 | 76.86(9) |
| Zn1-S1-Zn2 | 83.54(2) | Zn1-S3-Zn3 | 82.98(2) |
| Zn1-S2-Zn2 | 85.30(2) | Zn1-S3-Zn4 | 83.06(2) |

**Table 3.** Hydrogen bonds for $[Zn(Zn\mathbf{L})_2](ClO_4)_2 \cdot 2CH_3CN$ (**1c**) [Å and °].

| D-H...A | d(D-H) | d(H...A) | d(D...A) | <(DHA) |
|---|---|---|---|---|
| N(2)-H(2)...O(1)#1 | 1.00 | 2.08 | 3.018(3) | 155.4 |
| N(4)-H(4)...O(6) | 1.00 | 2.08 | 3.035(3) | 158.1 |
| N(6)-H(6)...N(10)#2 | 1.00 | 2.13 | 3.053(4) | 153.3 |
| N(8)-H(8)...O(5)#3 | 1.00 | 2.08 | 3.005(3) | 153.2 |

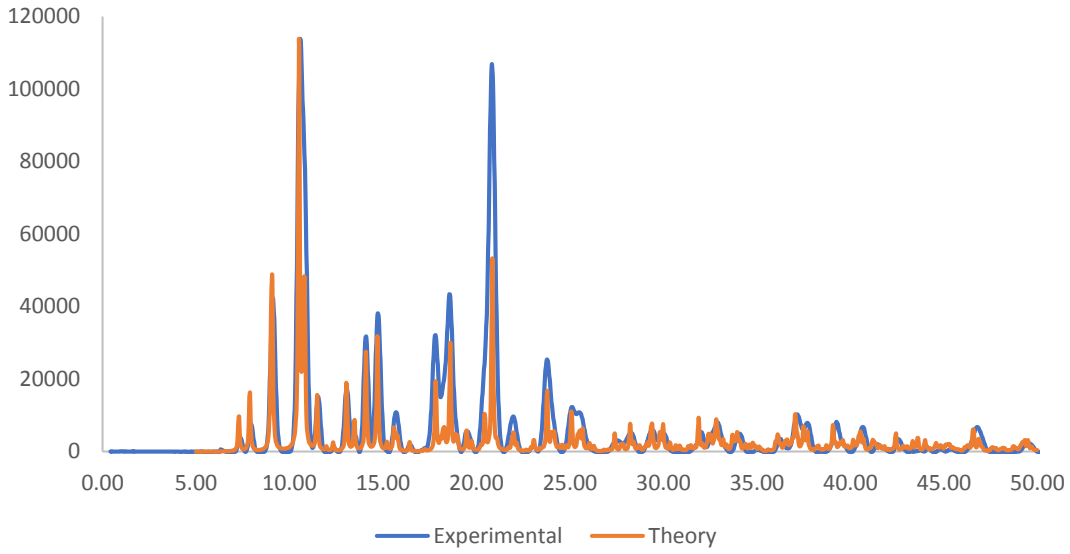


**Figure 14.** Comparison of theoretical and experimental powder patterns for **1c**

Mixed metal solvate $[Hg(ZnL_2)_2](ClO_4)_4 \cdot 2H_2O$ (**2a**) formed in the tetragonal space group *I*-4 and was a pseudo-isomorph of **1a′** with the perchlorates replacing the tetrafluoroborates and the mercury replacing the zinc as a metal center (Figure 15). In regard to symmetry, a crystallographic S4 was seen running through the three mercury atoms. Its asymmetric unit was composed of two one quarter $[Hg(Zn\mathbf{L})_2]^{2+}$ complex ions, a perchlorate ion, and a solvent water

molecule. The disordered perchlorate had two positions with two oxygens hydrogen bonded to N2 and the hydrogen on the water molecule (Figure 16, Table 4). This water molecule was also a hydrogen bond donor with S1 and as a hydrogen bond acceptor with N4 (Figure 16d, Table 5). It was found to be an independent meso (ΔΛ) complex; ions were arranged end-to-end with each other in continuous strands. The four-fold aryl embraces link the strands together along the c axis of the cell. Neighboring strands are offset by half their length creating one screw axis. The experimental powder pattern of crystalline samples of **2a** with uniform habit matched the calculated powder pattern extremely well (Figure 17). Furthermore, precipitates of **2** retaining water upon vacuum drying had a powder pattern similar to **2a** and an amorphous powder pattern if no water was retained. This corroborates the claim that **2a** is a pseudo-isomorph of **1a′** (Figure 15).

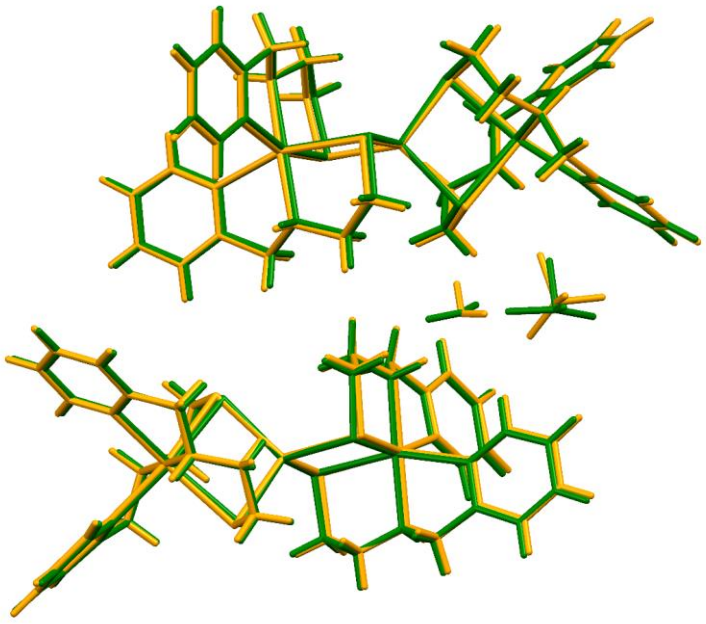

**Figure 15.** Mercury-calculated $M_3S_4$ overlays of the two independent molecules of **1a′** (green) and **2a** (orange).

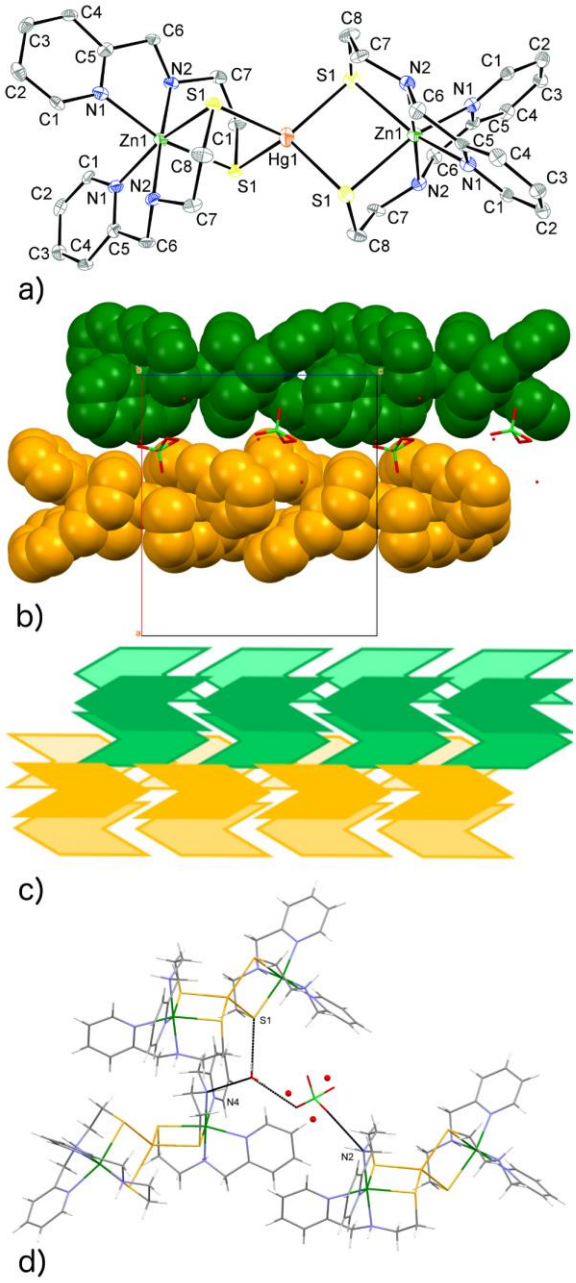


**Figure 16.** a) Framework of $[Hg(ZnL_2)_2](ClO_4)_4 \cdot 2H_2O$ (**2a**) with atom labeling b) Space filling diagram of **2a** to illustrate head-to-tail configuration of two pairs of complexes with the four-fold embrace outlined. c) Schematic packing diagram for **2a**. d) Outline of the hydrogen bonding occurring between the corresponding sulfur, amino, solvent molecules, and perchlorate groups of **2a**.

**Table 4.** Selected bond lengths (Å) and bond angles (º) for **2a**

| | molecule 1 | molecule 2 |
|---|---|---|
| Hg1-S1 | 2.528(4) | 2.543(3) |
| Zn1-S1 | 2.594(4) | 2.576(3) |
| Zn1-N1 | 2.169(11) | 2.234(10) |
| Zn1-N2 | 2.130(11) | 2.116(9) |
| S1-Hg1-S1′#1 | 93.20(15) | 95.54(14) |
| S1-Hg1-S1″#2 | 118.17(9) | 116.85(8) |
| S1-Zn1-S1′ S2-Zn2-S2#5 | 90.16(17) | 93.96(16) |
| S1-Zn1-N1 S2-Zn2-N3 | 160.0(3) | 159.4(2) |
| S1-Zn1-N2 S2-Zn2-N4 | 82.1(3) | 82.6(3) |
| S1-Zn1-N1′ | 92.9(3) | 92.7(2) |
| S1-Zn1-N2′ | 96.3(3) | 97.5(3) |
| N1-Zn1-N2 | 77.9(4) | 77.2(4) |
| N1-Zn1-N1′ | 91.0(5) | 87.7(5) |
| N1-Zn1-N2′ | 103.7(4) | 102.7(4) |
| N2-Zn1-N2′ | 177.7(6) | 179.8(5) |
| Hg1-S1-Zn1 | 88.32(11) | 85.25(10) |

**Table 5.** Hydrogen bonds for $[Hg(Zn\mathbf{L})_2](ClO_4)_2\ 2H_2O$ (**2a**) [Å and °].

| D-H...A | d(D-H) | d(H...A) | d(D...A) | <(DHA) |
|---|---|---|---|---|
| N(2)-H(2)...O(1A)#1 | 1.00 | 2.53 | 3.198(16) | 123.9 |
| N(2)-H(2)...O(3B)#1 | 1.00 | 2.34 | 3.23(3) | 147.6 |
| N(4)-H(4)...O(5)#2 | 1.00 | 1.92 | 2.859(14) | 155.7 |
| O(5)-H(1W)...S(1)#3 | 0.83(3) | 2.45(9) | 3.218(11) | 155(18) |
| O(5)-H(2W)...O(2A) | 0.83(3) | 2.08(7) | 2.87(5) | 162(15) |
| O(5)-H(2W)...O(2B) | 0.83(3) | 2.08(12) | 2.79(2) | 144(17) |

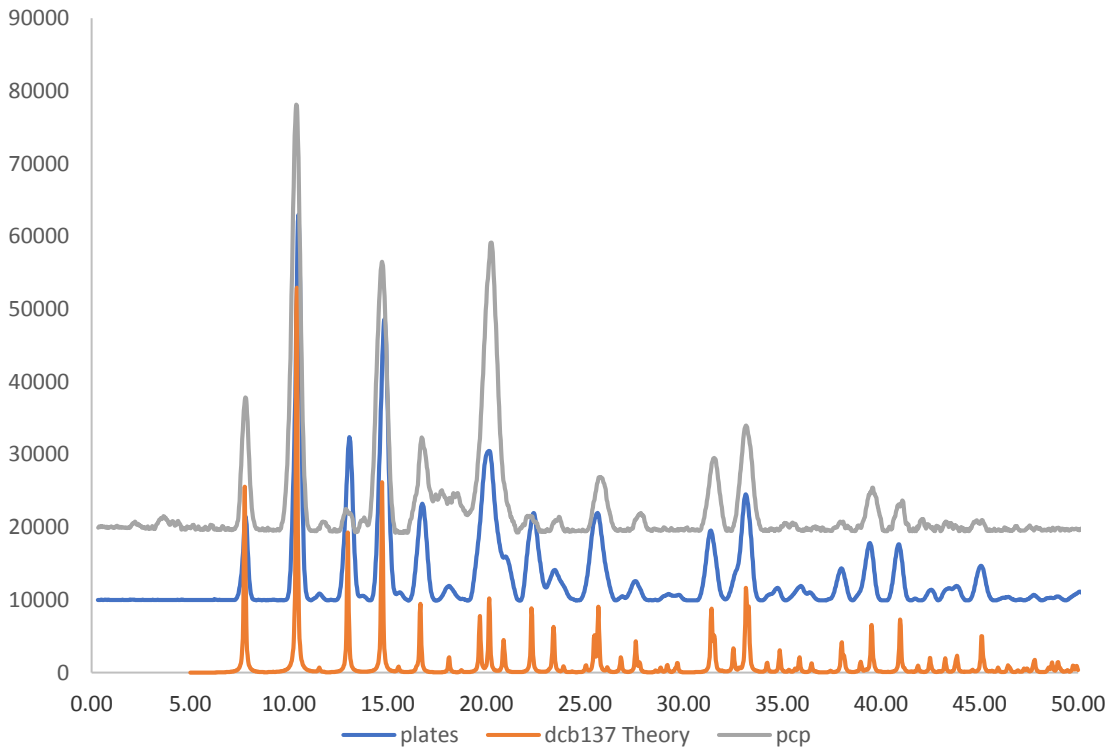


**Figure 17.** Comparison of theoretical and experimental powder patterns for **2a**.

The solvomorph $[Hg(ZnL_2)_2](ClO_4)_4 \cdot 2CH_3CN \cdot H_2O \cdot 0.5$toluene (**2d**) crystallized in the monoclinic space group, *C2/c*. A crystallographic C2 axis is present through the three central metal ions (Figure 18a). These complex ions were present as a racemic mixture of diastereomers, ($\Delta\Delta/\Lambda\Lambda$). The asymmetric unit contained one complex ion and a multitude of other solvent molecules: one ordered acetonitrile, one disordered acetonitrile sitting on a special position, two half waters, and a single toluene. Each perchlorate was bonded to two amine nitrogen, N2-N6 or alternatively N4-N8, thus resulting in hydrogen bonded stacks of pairwise alternative diastereomers in the ac plane (Figure 18c). Additionally, the complexes were aligned head-to-head with a toluene sequestered in between, or tail-to-tail with an acetonitrile located between. There was a considerable amount of π-π stacking interactions that occur between pyridyl rings. The N7 pyridyl rings displayed sandwiched π-π stacking, while the N3 and N5 pyridyl rings both had offset parallel π-π stacking interactions between them. Furthermore, there is also σ-π interactions between the N1 pyridyl rings and the toluene solvent molecules. This particular solvomorph was unstable to loss of solvent (Figure 18b). However, the 100K powder pattern of **2d** immediately after removal of the mother liquor was found to match a majority of the predicted peaks from the crystal structure (Figure 19). The additional peaks found in the powder pattern grew as the remaining solvent left and were not consistent with any of the other solvomorphs observed.

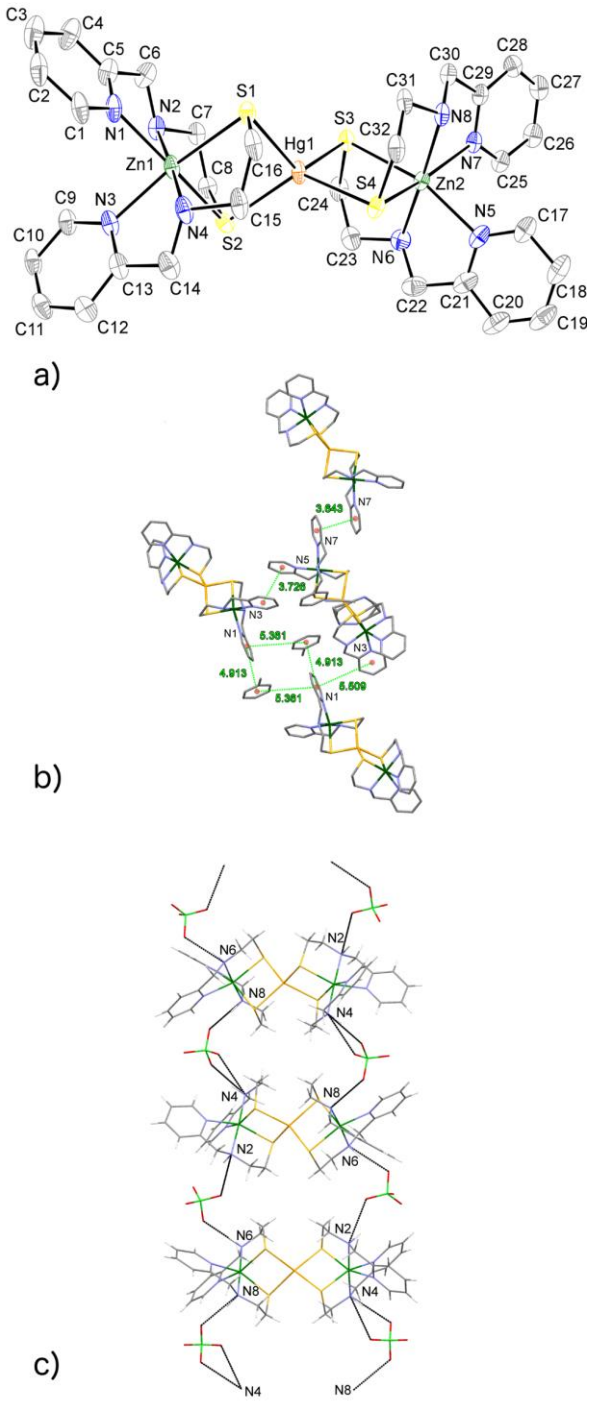


**Figure 18.** a) Framework of $Hg(ZnL_2)_2](ClO_4)_4 \cdot 2CH_3CN \cdot H_2O \cdot 0.5$toluene (**2d)** with atom numbering scheme. b) Pyridyl ring π-π stacking occurring in **2d**. c) Hydrogen bonding between the perchlorate and amino nitrogen groups of **2d**.

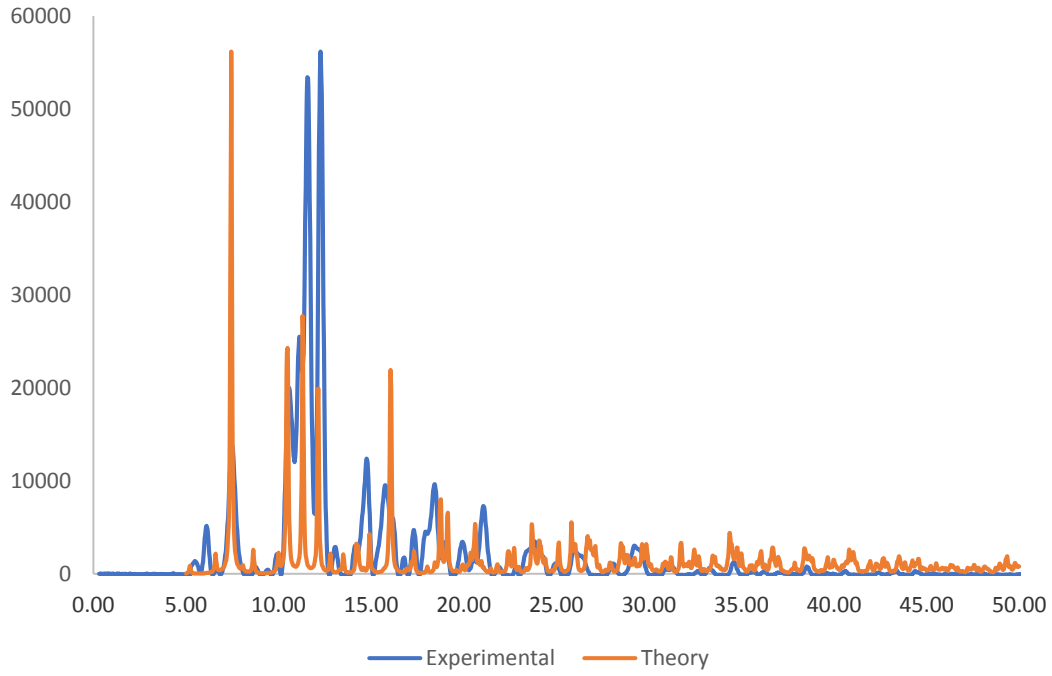


**Figure 19.** Comparison of theoretical and experimental powder patterns for **2d**.

Indirect methods provided solvate $[Hg(ZnL_2)_2](ClO_4)_2 \cdot CH_3CN \cdot 0.5$toluene (**2f**) in the triclinic space group P-1. Identical pseudo-meso ΔΛ molecules were arranged in head-to-tail strands linked together through four-fold aryl embraces (Figure 20b). The asymmetric unit of these clusters were made up of $[Hg(Zn\mathbf{L})_2]^{2+}$, two well-ordered perchlorates, an acetonitrile and half a toluene. Due to the way the perchlorates were situated within these units, the clusters were linked together through hydrogen bonding interactions between a bridging perchlorate and the amine hydrogen N2 (Figure 20d, Table 7). Additional hydrogen bonding formed a bridge between N4 and N8 of adjacent complexes involving the two oxygens of the second perchlorate

(Figure 20). The acetonitrile was aligned for hydrogen bonding with the remaining amino hydrogen on N6. The inversion related sheets form columnar stacking with the complex ions within the ab plane.

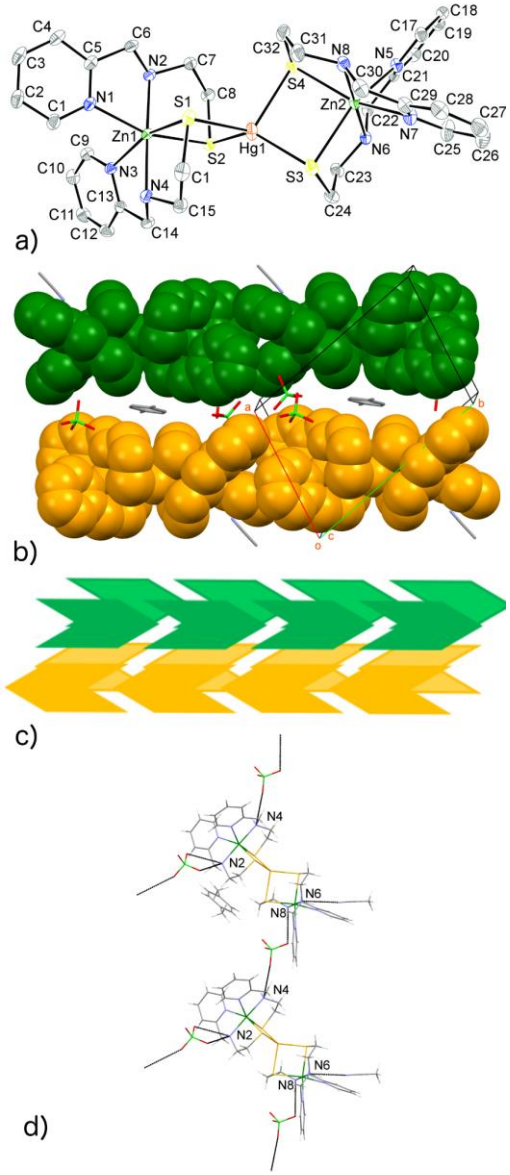


**Figure 20.** a) Framework of $[Hg(ZnL_2)_2](ClO_4)_2 \cdot CH_3CN \cdot 0.5$toluene (**2f)** with atom labeling. b) Space filling complex ion diagram of **2f** showing the head-to-tail arrangement of complexes with the four-fold aryl embraces outlined c) Schematic packing diagram of **2f**. d) Hydrogen bonding between complexes to illustrate packing interactions of **2f**.

**Table 6.** Selected bond lengths (Å) and bond angles (º) for **2f**

| | | | |
|---|---|---|---|
| Hg1-S1 | 2.5711(12) | Hg1-S3 | 2.4636(13) |
| Hg1-S2 | 2.4749(12) | Hg1-S4 | 2.5858(12) |
| Zn1-S1 | 2.5072(12) | Zn2-S3 | 2.5888(14) |
| Zn1-S2 | 2.5866(12) | Zn2-S4 | 2.5025(14) |
| Zn1-N1 | 2.205(4) | Zn2-N5 | 2.197(4) |
| Zn1-N2 | 2.156(4) | Zn2-N6 | 2.170(4) |
| Zn1-N3 | 2.219(4) | Zn2-N7 | 2.208(4) |
| Zn1-N4 | 2.160(4) | Zn2-N8 | 2.162(4) |
| S1-Hg1-S2 | 94.29(4) | S2-Hg1-S3 | 134.81(4) |
| S1-Hg1-S3 | 114.70(4) | S2-Hg1-S4 | 107.67(4) |
| S1-Hg1-S4 | 111.91(4) | S3-Hg1-S4 | 93.30(4) |
| S1-Zn1-S2 | 93.14(4) | S3-Zn2-S4 | 92.32(4) |
| S1-Zn1-N1 | 95.56(11) | S3-Zn2-N5 | 156.98(10) |
| S1-Zn1-N2 | 97.34(11) | S3-Zn2-N6 | 81.91(11) |
| S1-Zn1-N3 | 158.95(11) | S3-Zn2-N7 | 95.79(13) |
| S1-Zn1-N4 | 83.84(11) | S3-Zn2-N8 | 97.92(12) |
| S2-Zn1-N1 | 156.96(12) | S4-Zn2-N5 | 93.80(11) |
| S2-Zn1-N2 | 82.19(11) | S4-Zn2-N6 | 97.58(11) |
| S2-Zn1-N3 | 91.20(11) | S4-Zn2-N7 | 158.21(12) |
| S2-Zn1-N4 | 95.02(11) | S4-Zn2-N8 | 83.02(13) |
| N1-Zn1-N2 | 75.58(15) | N5-Zn2-N6 | 75.30(14) |
| N1-Zn1-N3 | 88.29(15) | N5-Zn2-N7 | 86.57(16) |
| N1-Zn1-N4 | 107.07(16) | N5-Zn2-N8 | 104.83(15) |
| N2-Zn1-N3 | 103.65(15) | N6-Zn2-N7 | 103.56(16) |
| N2-Zn1-N4 | 177.02(15) | N6-Zn2-N8 | 179.38(17) |
| N3-Zn1-N4 | 75.26(15) | N7-Zn2-N8 | 75.86(17) |
| Hg1-S1-Zn1 | 86.09(4) | Hg1-S3-Zn2 | 87.48(4) |
| Hg1-S2-Zn1 | 86.42(4) | Hg1-S4-Zn2 | 86.73(4) |

**Table 7.** Hydrogen bonds for $[Hg(Zn\mathbf{L})_2](ClO_4)_2 \cdot CH_3CN \cdot 0.5$ toluene (**2f**) [Å and

| D-H...A | d(D-H) | d(H...A) | d(D...A) | <(DHA) |
|---|---|---|---|---|
| N(2)-H(2)...O(1) | 1.00 | 2.23 | 3.061(6) | 139.3 |
| N(2)-H(2)...O(2) | 1.00 | 2.35 | 3.182(6) | 139.9 |
| N(4)-H(4)...O(6)#1 | 1.00 | 2.38 | 3.127(9) | 130.6 |
| N(6)-H(6)...N(9)#2 | 1.00 | 2.14 | 3.085(7) | 157.5 |
| N(8)-H(8)...O(5) | 1.00 | 2.24 | 3.216(7) | 164.7 |

Lastly, $[Hg(ZnL_2)_2](ClO_4)_2 \cdot 2CH_3CN$ (**2c**) was also formed through the indirect synthesis method, forming crystals in the monoclinic space group P2/*n* (Figure 21). These complexes were not isomorphic with **1c**, as a crystallographic C2 axis ran through the three metal ions of the complex. The asymmetric unit consisted of a well- ordered perchlorate, a disordered acetonitrile sitting in a special position, and one half of the pseudo-meso (ΔΛ) complex ion. These complexes were arranged in a head-to-tail fashion, forming continuous strands along the b axis of the cell through the four-fold aryl embraces. The inversely related complexes formed alternating stacks within the ac plane of the cell. Hydrogen bonding was seen between the oxygen of perchlorates and the amino nitrogens N2 and N4 forming bridges between the complexes (Figure 21d).

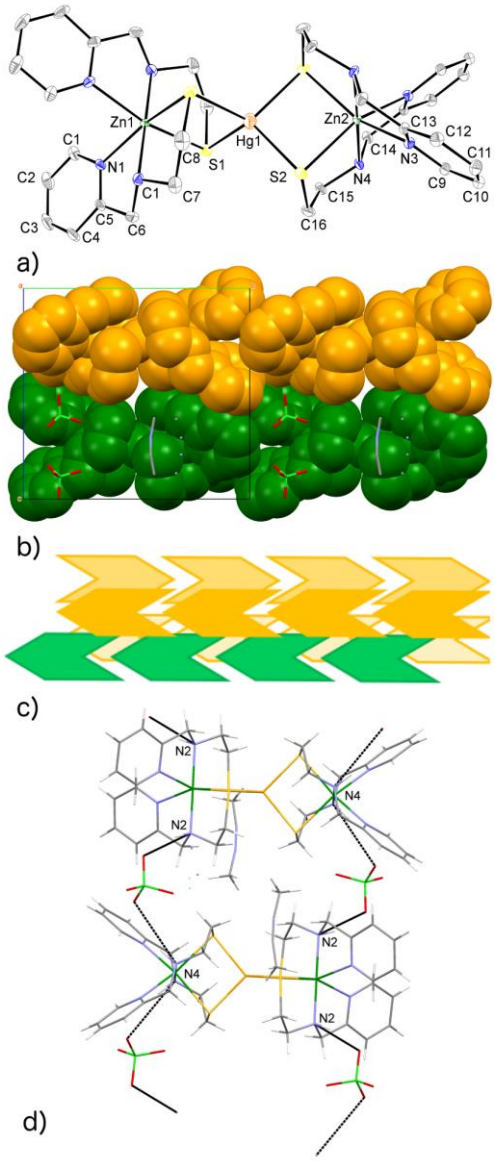


**Figure 21.** a) Framework of $[Hg(ZnL_2)_2](ClO_4)_2 \cdot 2CH_3CN$ (**2c)** with atom labeling b) Space filling complex ion diagram of **2c** illustrating the head-to-tail structure of the two pairs of inversely related complexes with the four-fold aryl embrace outlined. c) Schematic packing diagram of **2c**. d) Hydrogen bonding interactions illustrated between the perchlorate and amino groups of **2c**.

**Related work with mixed N,S donor ligands**

In a related project, our lab has been studying the Group 12 coordination chemistry of mixed N,S donor ligand N-(2-pyridylmethyl)-N-(2-(methylthio)ethyl)-N-(2-thioethyl)-amine (**L′**) (Figure 4). In the presence of base, $Cd(ClO_4)_2$ and air, a complex of **L′** with composition $[Cd_6\mathbf{L'}_6(CO_3)_4](ClO_4)_2$ forms. The carbonate in this unusual complex comes from carbon dioxide in the air. Since known forms of the metalloenzyme carbonic anhydrase use either Zn(II) or Cd(II) to promote related carbon dioxide chemistry, the Zn(II) coordination chemistry of **L′** was investigated. Based on DFT calculations performed by Professor Craig Bayse in the Department of Chemistry and Biochemistry at Old Dominion University, a comparable complex of zinc was expected to be stable.

Attempts to form a zinc carbonate complex from air or $CO_2$ saturated solutions of $Zn(ClO_4)_2$, base, and **L′** were unsuccessful. Analysis of these reaction mixtures by ESI-MS provided no evidence for the formation of the ions expected for the desired carbonate complex. However, an unusual complex with the composition $[(\mathbf{L'})_4Zn_5(\mu\text{-}OH_2)](ClO_4)_4$ (**4**) was isolated (Figure 22). The Zn metal center is tetrahedrally coordinated, with Zn-S-Zn bonds at the core.

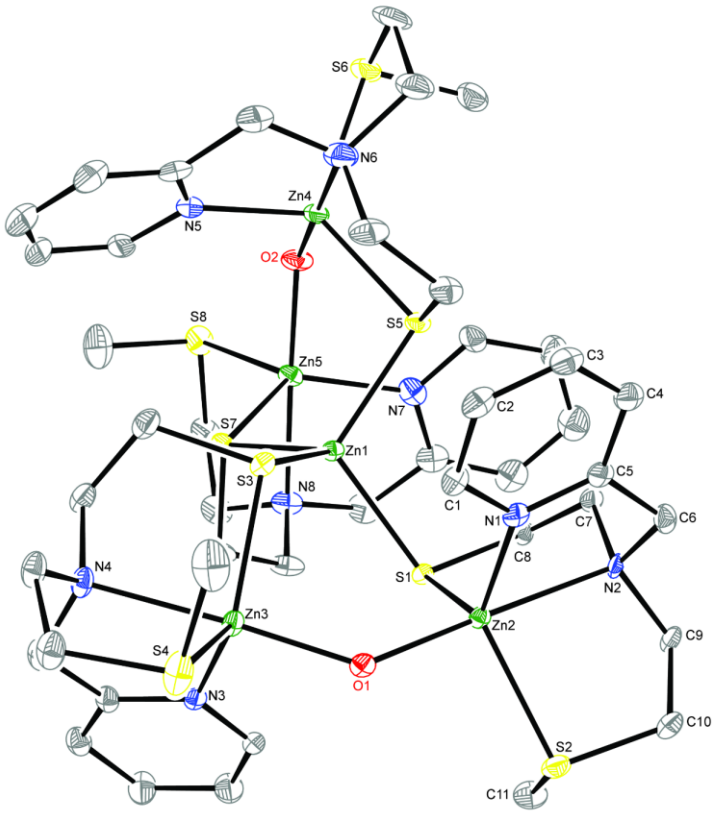


**Figure 22.** ORTEP diagram of $[(\mathbf{L'})_4Zn_5(\mu\text{-}OH_2)](ClO_4)_4$ (**4**)

Interestingly, the only other structurally characterized spiro bicycle [5.5] complex is $[(Py_2S)_4Fe_5(\mu\text{-}OH_2)]\ (BF_4)_4$ (**5**) (Figure 23).[19]

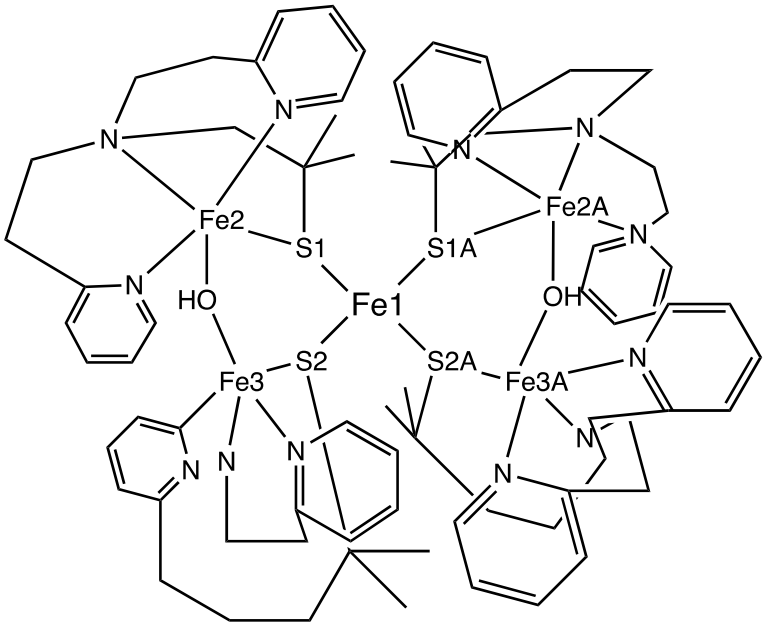


**Figure 23.** ChemDraw sketch of complex **5** (complex has a 4+ charge).[20]

Krishnamurthy et al. prepared the iron complex because of their interest in transition metal thiolate complexes and their relationship to polynuclear and mononuclear metalloenzyme sites. They chose a polydentate ligand to model biologically relevant cysteinate ligation because of the established synthetic challenges associated with controlling thiolate coordination. Through aprotic conditions (THF) and almost stoichiometric amounts of water, this hydroxide containing structure was synthesized. Krishnamurthy et al. noted that their "dinuclear, face-sharing bioctahedral complex with an unusual set of single atom bridging groups compromising of two thiolate S atoms and one hydroxide atom" had no literature counterpart. Complex **4** provides a second example of this unusual architecture (Figure 8). Notable differences between complexes **4** and **5** include: the metal center in **4** was more tetrahedral in shape while **5** was reported to have a distorted tetrahedral coordination center. The bond angles of **5** with regards to the S-Fe-S bonds: S1-Fe1-S1 (116.79°), S1-Fe1-S2 (116.13°), S1-Fe1-S2 (94.18°), and S2-Fe1-S2 (121.36°)

as well as an average bond length of 112° indicate a distorted tetrahedral configuration.[19] The Zn-S-Zn bond angles of complex **4**: S7-Zn1-S1 (111.88°), S7-Zn1-S5 (107.90°), S1-Zn1-S5 (109.56°), S7-Zn1-S3 (107.78°), S1-Zn1-S3 (107.38°), and S5-Zn1-S3 (112.47°) as well as an average bond length of 109° were indicative of a more traditional tetrahedral coordination center (Table 9).

**Table 8**. Crystallographic data for $[Zn((Zn(\mathbf{L}))_2(\mu\text{-}OH))_2](ClO_4)_4 \cdot H_2O$ (**4**)

| | |
|---|---|
| Empirical Formula | $C_{44}H_{72}Cl_4N_8O_{19}S_8Zn_5$ |
| Formula mass [g mol$^{-1}$] | 1742.22 |
| Crystal Size [mm] | 0.43 × 0.25 × 0.13 |
| Crystal System | Orthorhombic |
| Space Group | *Pca*2$_1$ |
| *a*[Å] | 25.1797(4) |
| *b*[Å] | 13.2796(2) |
| *c*[Å] | 22.7405(3) |
| α[°] | 90 |
| β[°] | 90 |
| γ[°] | 90 |
| V[Å$^3$] | 7603.89(19) |
| Z | 4 |
| Radiation (monochromatic) | Cu Kα |
| λ [Å] | 1.54178 |
| T [K] | 100(2) |
| $\rho_{calc}$ [g cm$^{-3}$] | 1.522 |
| μ [mm$^{-1}$] | 5.646 |
| Measured reflections | 86173 |
| Ind. reflections [$R_{(int)}$] | 13200 [R(int) = 0.0524] |
| Completeness | 100% (θ = 67.000°) |
| Data / restraints / parameters | 13200 / 844 / 803 |
| R1[a], wR2[b] [$I>2\sigma(I)$] | 0.0668, 0.1959 |
| R1[a], wR2[b] (all data) | 0.0680, 0.1985 |
| Goodness-of-fit (GOF) | 1.075 |

[a] $R1 = \Sigma||F_o| - |F_c||/\Sigma|F_o|$, and $S = [\Sigma[w(F_o^2 - F_c^2)^2]/(n - p)]^{1/2}$ ; [b] $wR2 = [\Sigma[w(F_o^2) - (F_c^2)]^2/\Sigma[w(F_o^2)^2]^{1/2}$

**Table 9.** Selected interatomic distances (Å) and angles (°) in $[Zn((Zn\mathbf{L})_2(\mu\text{-}OH))_2](ClO_4)_4\ H_2)$ (**4**)

a) Central Zinc

| | | | |
|---|---|---|---|
| Zn1-S1 | 2.341(3) | Zn1-S3 | 2.351(3) |
| Zn1-S5 | 2.343(3) | Zn1-S7 | 2.338(3) |
| S1-Zn1-S3 | 107.30(10) | S3-Zn1-S5 | 112.47(11) |
| S1-Zn1-S5 | 109.56(10) | S3-Zn1-S7 | 107.78(11) |
| S1-Zn1-S7 | 111.88(11) | S5-Zn1-S7 | 107.90(11) |

b) Terminal Zinc

| $Zn_n$ | Zn2 | Zn3 | Zn4 | Zn5 |
|---|---|---|---|---|
| $Zn_n$-$N_{py}$ | 2.079(9) | 2.053(10) | 2.056(12) | 2.064(11) |
| $Zn_n$-$N_{am}$ | 2.296(9) | 2.278(9) | 2.288(12) | 2.307(10) |
| $Zn_n$-$S_{in}$ | 2.356(3) | 2.360(3) | 2.354(3) | 2.342(3) |
| $Zn_n$-$S_{Me}$ | 2.472(3) | 2.493(3) | 2.455(3) | 2.437(3) |
| $Zn_n$-O | 1.988(7) | 1.976(8) | 1.961(9) | 1.993(8) |
| $N_{py}$-$Zn_n$-$N_{am}$ | 77.3(3) | 78.5(4) | 77.9(5) | 78.3(4) |
| $N_{py}$-$Zn_n$-$S_{in}$ | 119.1(3) | 120.8(2) | 122.5(4) | 124.5(3) |
| $N_{py}$-$Zn_n$-$S_{Me}$ | 126.0(3) | 119.3(3) | 110.8(3) | 115.3(3) |
| $N_{py}$-$Zn_n$-O | 100.9(3) | 99.4(3) | 102.4(5) | 99.7(4) |
| $N_{am}$-$Zn_n$-$S_{in}$ | 85.4(2) | 84.8(3) | 84.3(3) | 84.8(3) |
| $N_{am}$-$Zn_n$-$S_{Me}$ | 81.9(2) | 82.9(2) | 82.6(3) | 82.9(3) |
| $N_{am}$-$Zn_n$-O | 176.6(3) | 177.3(4) | 179.6(4) | 177.3(4) |
| $S_{in}$-$Zn_n$-$S_{Me}$ | 107.93(11) | 114.21(13) | 120.55(12) | 114.36(11) |
| $S_{in}$-$Zn_n$-O | 97.9(2) | 97.8(2) | 95.7(3) | 97.9(3) |
| $S_{Me}$-$Zn_n$-O | 97.0(2) | 96.7(2) | 97.1(3) | 96.3(3) |
| $Zn_n$-$S_{in}$-Zn1 | 105.70(10) | 106.90(10) | 104.70(10) | 103.40(10) |

When taking an NMR of this complex, it was expected to be in a single $H_a$ environment at cryogenic temperatures, however it turned out to be much more complicated than that. Variable temperature proton NMR shows multiple environments in slow exchange on the chemical shift time scale at low temperatures and a single exchange averaged environment at elevated temperatures (Figure 27). The temperature-dependent behavior of the $H_a$ doublet suggests at least four complexes in slow exchange on the chemical shift time scale at at -40 °C. One $H_a$ environment at 8.66 ppm, labeled as d, one $H_a$ environment at 8.73 ppm, labeled as c, three $H_a$ in equal proportion at 8.30, 8.87, and 9.20 ppm, labeled as a, and the two $H_a$ in equal proportion at 6.62 and 8.75 ppm, labeled as b (Figure 26). Based on precedent literature, we are suggesting that environment a is $[Zn_5\mathbf{L'}_6](ClO_4)$ as it is similar to the NMR data of $[Hg_5\mathbf{L'}_6](ClO_4)$.[11] Environment b or c could correspond to **4**. The remaining environments are suggested to correspond to either a dimer or tetramer of Zn**L**′ (Figure 24). Note that a tetramer of Zn**L**′ has several possible conformers, some of which could give rise to two ligand environments in slow exchange (Figure 25).

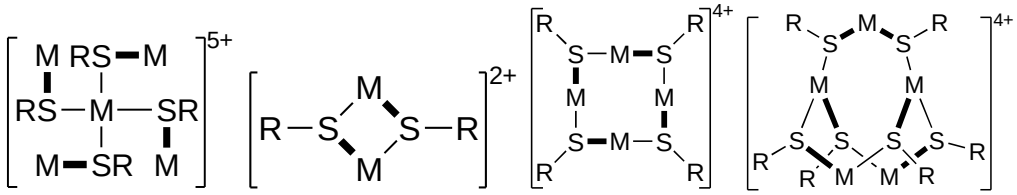


**Figure 24.** Possible molecular multimuclear complexes seen in $H_a$ environment of complex **4**

A $(Hg\mathbf{L'})_4$ macrocycle (**6**) has been prepared previously in our lab.[20] Complex **6** crystallizes in the boat-boat shown in Figure 25. Other potential conformers were suggested by variable temperature NMR studies.

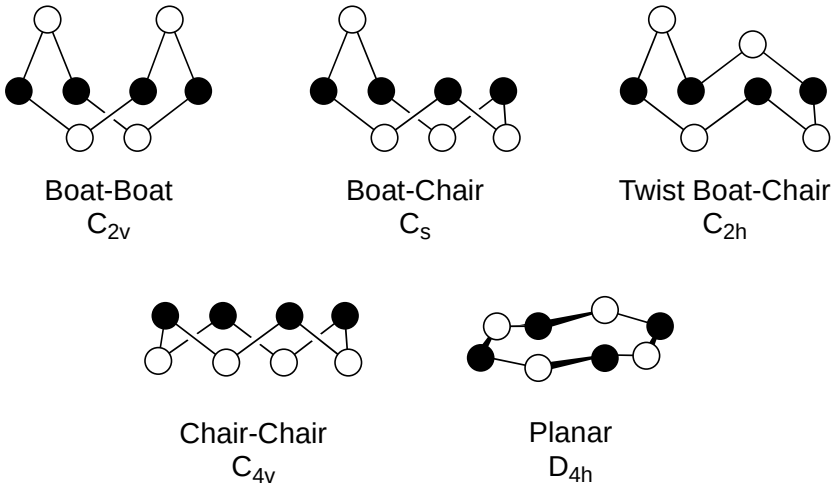


**Figure 25.** Possible conformers of the $[(\mathbf{L'})_4Zn_5(\mu\text{-}OH_2)](ClO_4)_4$ complex

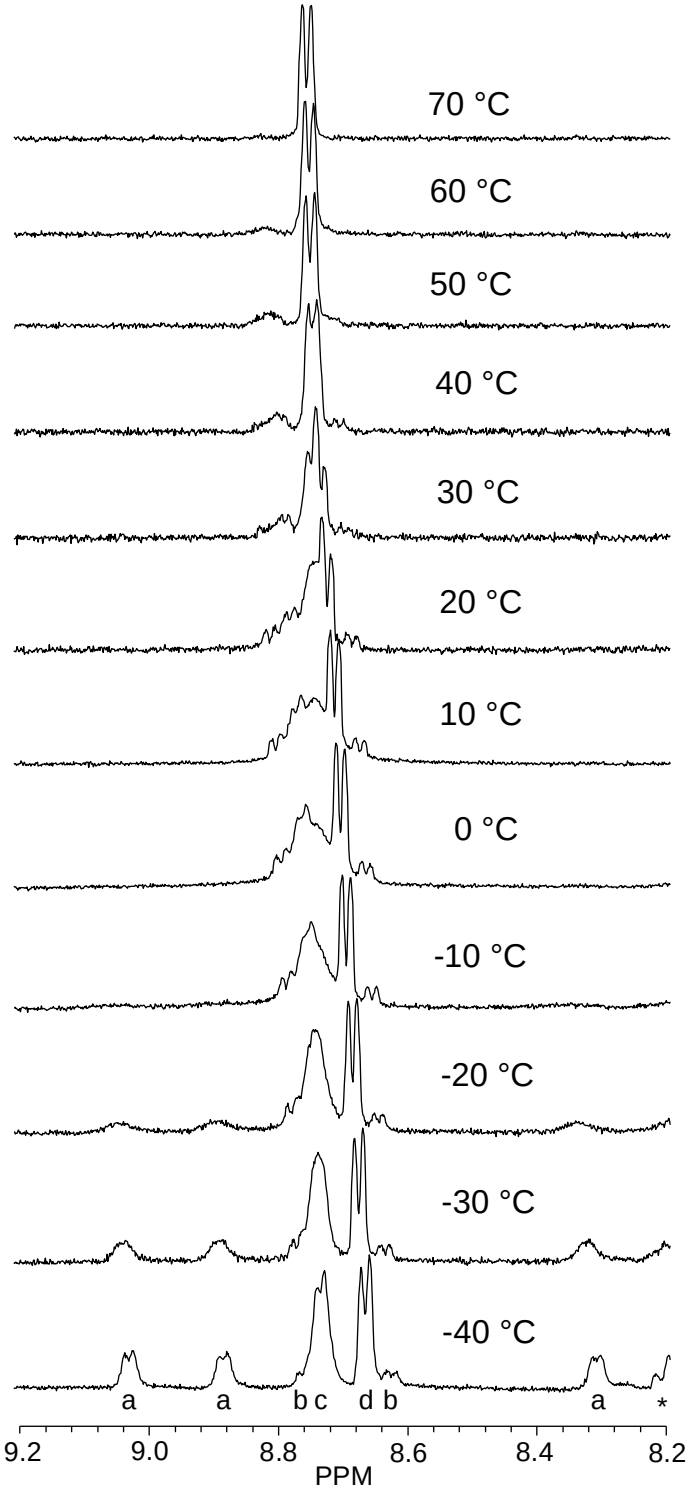


**Figure 26.** Methylene portion of variable temperature proton NMR experiment on **4**, asterisk indicates peak for different ligand proton ($H_c$) moving into this region with decreasing temperature, a,b,c, and indicate the different environments of $H_a$

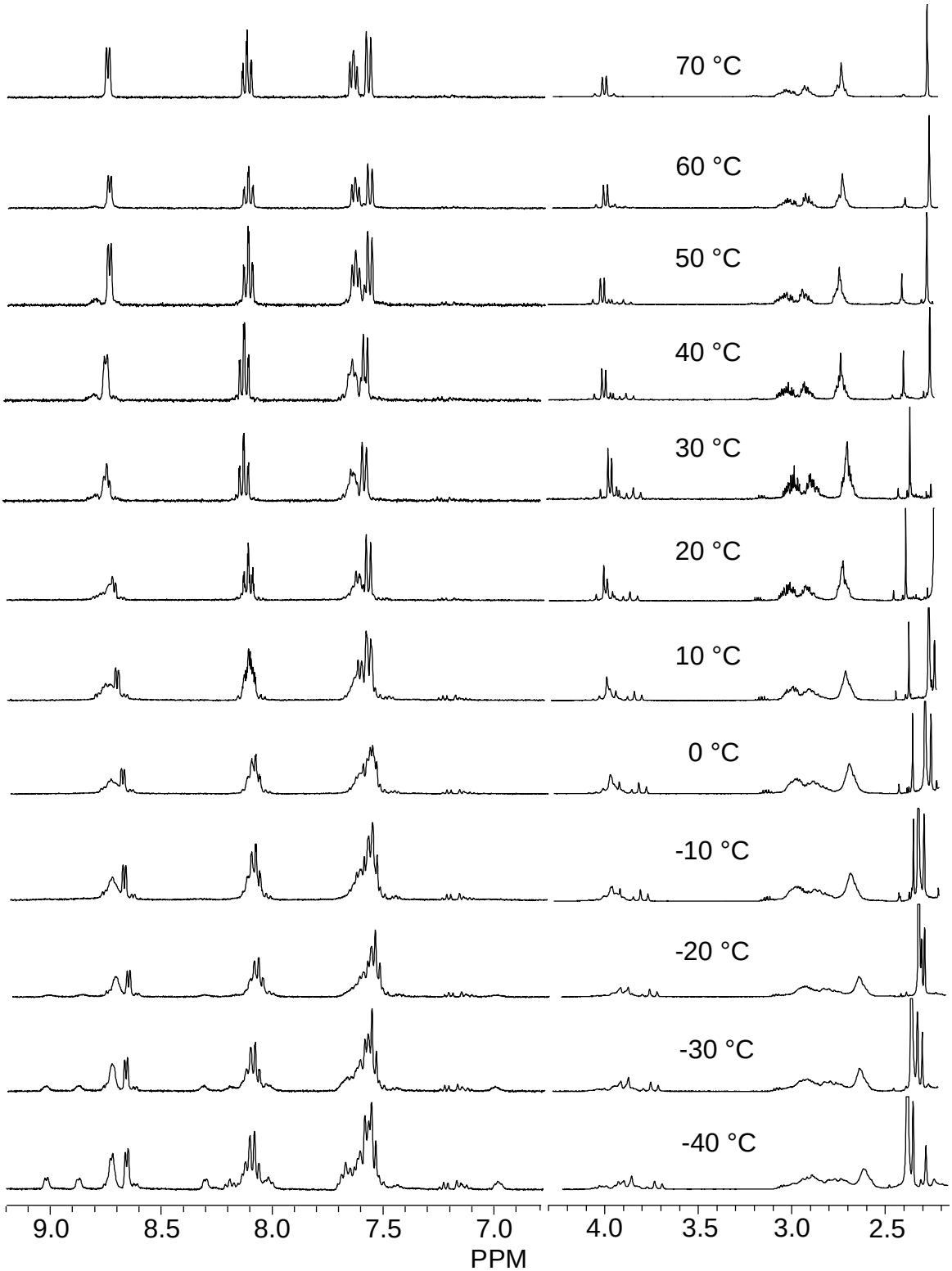


**Figure 27.** Variable temperature proton NMR experiment on **4**, aromatic region of spectra has been enlarged to show detail.

## Conclusion

This research has focused on the preparation and characterization of novel multinuclear complexes of Group 12 metals and mixed N,S donor ligands. Both ligands investigated formed thiolates upon deprotonation that served as bridges between two metal ions in each of the complexes prepared. The two or three remaining ligand donors were bound to the same metal ion as the thiolate in structurally characterized complexes, resulting in the formation of molecular complexes rather than the polymeric materials that plague the coordination chemistry of Group 12 metal ions with simple thiolates.

Formation of the first alkyl-thiolate-bridged mixed metal complex $[Hg(Zn\mathbf{L})_2](ClO_4)_2$ (**2**) was shown by both directly and indirectly, corroborated by X-ray crystallography, ESI-MS, and variable temperature solution state $^1$H NMR experiments. Notably, one of the complexes made, **2**·$2H_2O$ (**2a**), was pseudoisomorphic with the homometallic zinc complex $[Zn(Zn\mathbf{L})_2](BF_4)_2\cdot 2H_2O$ (**1a′**) suggesting Hg(II)-Zn(II) exchange can occur in Zn-metallothionein with preservation of overall structure. Furthermore, structural characterization of five $_{\text{solvates}}$ of **2** in a variety of different space groups with varying stereochemistry at the meridional octahedral Zn(II) centers is consistent with the known fluxionality of metallothionein. These novel synthetic mixed metal complexes complement protein studies permitting detail structural characterization that has proved elusive for any form of Hg(II) metallothionein to date.

In related work with tetradentate **L′**, pentanuclear $[Zn((Zn\mathbf{L}')_2(\mu\text{-}OH))_2](ClO_4)_2$ (**4**) was characterized by X-ray crystallography and and variable temperature solution state $^1$H NMR experiments. Based on parallels between the Zn(II) and Cd(II) forms of carbonic anhydrase and previous studies demonstrating that **L′** and $Cd(ClO_4)_2$ are able to fix carbon dioxide as carbonate, a carbonate complex had been the synthetic target of this synthesis. ESI-MS studies provided no

evidence for formation of the desired complex or likely precursors. While unexpected, complex **3** proved to be only the second example of a metal complex with spiro[5.5] core. Variable temperature $^{1}$H NMR characterization indicated that **3** crystallized from a solution containing several different Zn(II) complexes of **L′**. Preliminary results in the Bebout lab indicate the Hg(II) coordination chemistry of **L′** shares similar features. This project is ongoing in the Bebout lab.

In conclusion, mixed N,S donor ligands have provided access to unusual molecular complexes of Group 12 metal ions. Detailed characterization of new complexes using solid, solution and gas phase methods has enhanced understanding of similarities and differences in metal-dependent behavior.

## References


[1] Dudev, T.; Lim, C. *Chemical Reviews*, **2014**, *114*(1), 538–556.
[2] Gomes, C. C. A. M.; Wittung-Stafshede, P. *Protein folding and metal ions: mechanisms, biology and disease*; CRC Press: Boca Raton, **2011**.
[3] Nastri, F.; Chino, M.; Maglio, O.; Bhagi-Damodaran, A.; Lu, Y.; Lombardi, A. *ChemInform*, **2016**, *47*(44).
[4] Faller, P. *FEBS Journal*, **2010**, *277*(14), 2921–2930.
[5] Blindauer, C. A. *Journal of Inorganic Biochemistry*, **2008**, *102*(3), 507–521.
[6] Henkel, G.; Krebs, B. *Chemical Reviews*, **2004**, *104*(2), 801–824.
[7] Melis, K. A.; Carter, D. C.; Stout, C. D.; Winge, D. R. *Environmental Health Perspectives*, **1984**, *54*, 105–109.
[8] Li, Y.; Fan, Y.; Zhao, J.; Xu, X.; Jing, H.; Shang, L.; Gao, Y.; Li, B.; Li, Y.-F. *BioMetals*, **2016**, *29*(5), 893–903.
[9] Tang, X.; Wang, Y.-S.; Xue, J.-H.; Zhou, B.; Cao, J.-X.; Chen, S.-H.; Li, M.-H.; Wang, X.-F.; Zhu, Y.-F.; Huang, Y.-Q. *Journal of Pharmaceutical and Biomedical Analysis*, **2015**, *107*, 258–264.
[10] Pedrero, Z.; Ouerdane, L.; Mounicou, S.; Lobinski, R.; Monperrus, M.; Amouroux, D. *Metallomics*, **2012**, *4*(5), 473.
[11] Viehweg, J. A.; Stamps, S. M.; Dertinger, J. J.; Green, R. L.; Harris, K. E.; Butcher, R. J.; Andriole, E. J.; Poutsma, J. C.; Berry, S. M.; Bebout, D. C. *Dalton Transactions*, **2010**, *39*(13), 3174.
[12] Brand, U.; Vahrenkamp, H. *Inorganic Chemistry*, **1995**, *34*(12), 3285–3293.
[13] Mikuriya, M.; Jian, X.; Ikemi, S.-I.; Kawahashi, T.; Tsutsumi, H. *Bulletin of the Chemical Society of Japan*, **1998**, *71*(9), 2161–2168.
[14] Madeline Nestor, Thesis, William and Mary, **2011**
[15] Arici, C.; Sari, M.; Atakol, O.; Fuess, H.; Svoboda, I. *Main Group Metal Chemistry*, **2001**, *24*(4).
[16] Rombach, M.; Vahrenkamp, H. *European Journal of Inorganic Chemistry*, **2002**, *2002*(8), 2022–2025.
[17] Raymon, K. *Chemical and Engineering News*. Washington, D.C.
[18] Lai, W.; Berry, S. M.; Kaplan, W. P.; Hain, M. S.; Poutsma, J. C.; Butcher, R. J.; Pike, R. D.; Bebout, D. C. *Inorganic Chemistry*, **2013**, *52*(5), 2286–2288.
[19] Krishnamurthy, D.; Sarjeant, A. N.; Goldberg, D. P.; Caneschi, A.; Totti, F.; Zakharov, L. N.; Rheingold, A. L. *Chemistry - A European Journal*, **2005**, *11*(24), 7328–7341.
[20] Wei Lai, Thesis, William and Mary, **2005**